Forced vibration analysis of composite beams with piezoelectric layers based on the variable separation method

María Infantes, Philippe Vidal, Rafael Castro-Triguero, Laurent Gallimard, Olivier Polit

María Infantes, Philippe Vidal, Rafael Castro-Triguero, Laurent Gallimard, Olivier Polit. Forced vibration analysis of composite beams with piezoelectric layers based on the variable separation method.

Composite Structures, Volume 273 (2021)

https://doi.org/10.1016/j.compstruct.2021.114248

1. Introduction

Recently, it should be noted an increasing interest towards high-performance structures involving multifunctionality capabilites, as it has been pointed out in [1]. Not only structural but also non-structural functions represent the key issue in the develepment of such smart structural components. Electrical and thermal conductivity, sensing and actuation, energy harvesting and storage, self-healing, electromagnetic interference shielding, recyclability or biodegradability are some of the most promising multifunctionality capabilities [2]. An overview on the topics of smart structures can be found in [3,4]. As they will be involved in the present work, piezoelectric materials permit to convert mechanical and electrical energy at frequency ranges. Among others, structural health monitoring, active vibration damping, rapid shape adaptation or energy harvesting [5] are only some feasible applications of such smart piezoelectric components. Due to the complex manufacturing of such structural devices, a reliable numerical analysis tool is necessary to capture all the relevant phenomena that guide the design process. Some examples of recent numerical studies regarding the electro-mechanical analysis of piezoelectric energy harvesters are shown in [6–8]. Furthermore, if optimization processes and runtime control algorithms are addressed, the numerical simulation tool should be as robust and efficient as possible.

Various mathematical models developed for structures containing piezoelectric sensors and actuators can be classified into two broad categories including induced strain models and coupled electromechanical models. An overview on the modeling of piezoelectric structures is given in [4,9–12]. On the one hand, the induced strain models use approximate theories in order to incorporate external forces associated with the piezoelectric actuators. The electric potential is neglected as a state variable in the formulation; therefore these models cannot capture the coupled mechanical and electrical responses and are only limited to predict the actuator behavior of piezoelectric materials ([13–16]). On the other hand, the coupled electromechanical models provide a more consistent representation of both the sensor and actuator responses of piezoelectric materials, incorporating both the displacements and the electric potentials as the state variables in the formulation. Piezoelectric three-dimensional (3D) finite elements have been early proposed in [17–19]. However, the cost of 3D analysis becomes prohibitive when piezoelectric layers are thin compared to the structure size.

In order to overcome these restrictions, several theories for laminated structures including piezoelectric elements have been developed in the literature. A layerwise description is commonly used for the piezoelectric part (see [20]), therefore, the discussion concerns only the mechanical approach. The following classification is associated

with the dependence on the number of mechanical degrees of freedom (DOFs) with respect to the number of layers:

- The equivalent single layer approach (ESL): the number of unknowns is independent of the number of layers, but continuity of transverse shear and normal stresses is often violated at layer interfaces. This approach is called "hybrid" or "mixed" in the literature. We can distinguish classical laminate theory (CLT), first-order shear deformation theory FSDT [21–23] and higher-order theories. In the latter, the third-order shear deformation theory has been carried out in [24–27]. Other types of functions can be also considered as in [28] (exponential function). See also a refined Reissner–Mindlin approach taking into account the stretching effect [12].
- The layerwise approach (LW): the number of DOFs depends on the number of layers. This theory aims at overcoming the ESL shortcoming of allowing discontinuity of out-of-plane stresses on the interface layers. See for instance [29,30] for beams, [31–35] for plates, and [36] for shells. Note that an extensive assessment has been provided by Saravanos and Heyligher [10].

In this framework, refined models have been developed in order to improve the accuracy of ESL models while avoiding the computational burden of the LW approach. Starting from a refined layerwise description, some physical considerations can be introduced. Then, after some algebraic transformations, the number of unknowns becomes independent of the number of layers. This type of approach has been carried out in [37]. The resulting model can be classified as a zig-zag one (see the historical review of [38]). In the framework of electromechanical problems, Oh and Cho [39] have extended the third order zig-zag model. Note also the works of Kapuria for beams [40,41] and plates [42].

Finally, the so-called advanced models based on PVD or RMVT and CUF (Carrera Unified Formulation) must be referred here. Different types of interlaminar continuity can be considered: transverse shear/normal stresses and/or transverse electric displacement. For the works related to multilayered piezoelectric structures, readers can refer to [43,44] for plates and [11] for shells.

A promising alternative approach to reduce the computational cost in the field of the reduced-order modeling is based on the separation of variables [45]. It has been proposed in [46] with a Navier-type solution for the modeling of composite plates with a in-plane/ out-of-plane coordinates separation. Such variable separations have been successfully applied to composite structures in static case [47,48]. The forced vibration problem of composite beams subjected to harmonic excitation has also been considered previously by the authors of this study by using the Proper Generalized Decomposition framework [49]. In the latter reference, the displacements are written under the form of separated variable representation, i.e. a sum of products of unidimensional functions of x and z coordinates. The load frequency ω was introduced into the formulation as another problem variable, in order to achieve a more robust formulation. The aim of the present paper is to extend the previously developed method to laminated and sandwich beams with piezoelectric layers. Therefore, a multifield analysis of advanced composite structures is addressed, especially dedicated to the consideration of electro-mechanical coupling. Analogously, herein both displacements and electric potential are written under the form of a sum of products of x functions, z functions and load frequency functions. The deduced explicit solution allows us to avoid numerous classical computations for each discretized value of the load frequency in the study domain. To achieve that, the approximation of the 2D beam is based on a quadratic finite element (FE) approximation for the variation with respect to x and a quadratic LW description for the variation with respect to z. The electric unknowns are interpolated with a second-order expansion. Using the PGD, each unknown function of x is classically approximated using one degree of freedom (dof) at the node of the mesh while the LW unknown functions of z are global for the whole beam. Finally, the deduced non-linear problem implies the resolution of three 1D linear problems alternatively. This process yields to few unknowns involved in each of these linear problems.

The manuscript is organized as follows. First, the electromechanical formulation is recalled. Then, the particular assumption on the displacements and the electric potential is introduced. It leads to a non-linear problem to be solved. An iterative process based on a classical fixed point strategy allows us to obtain the coupling solution. In this process, three 1D linear problems described in the present work, have to be solved. The FE discretization is also given. Numerical evaluations are subsequently presented. A convergence study of the proposed algorithm is first conducted. Several numerical tests with wide range of slenderness ratios under various boundary conditions are considered in order to assess the validity of the method. The results in terms of modal parameters and frequency response functions are compared with exact elasticity solution and finite element simulations from a commercial FE software.

2. Reference problem description

In the present study, a composite beam of length L and thickness h is considered. The beam consists of NC layers assumed to be orthotropic in the beam axes. In addition, some of the layers are assumed to present a piezoelectric behavior. The beam is considered in the (x, z) plane, i.e., in the domain $\Omega = \Omega_x \times \Omega_z = [0 \leqslant x \leqslant L] \times \left[-\frac{h}{2} \leqslant z \leqslant \frac{h}{2}\right]$. The x axis is taken along the longitudinal beam axis whereas the z axis is taken along the thickness direction. The reader can refer to Fig. 1, where the striped areas represent layers of piezoelectric material. The main notation used throughout the present formulation is also given in Table 1.

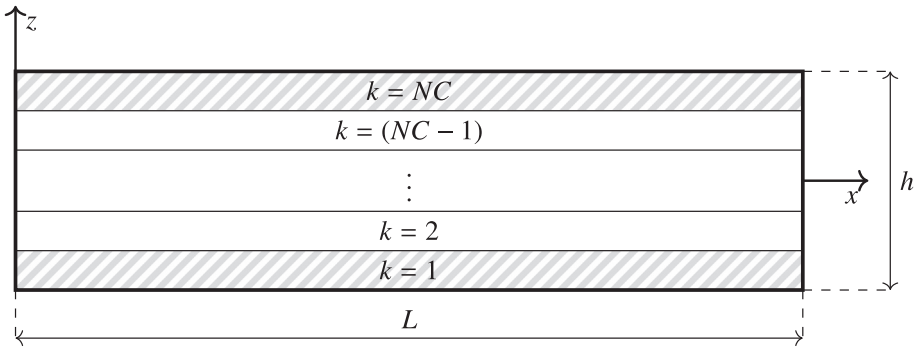

Fig. 1. The laminated beam with embedded piezoelectric layers and coordinate system.

Table 1
List of principal notation.

Ω_x	Domain in beam axis direction	NC	Number of layers
Ω_z	Domain in thickness direction	N	Number of total enrichment steps
ω	Load frequency	$[q^v], [q^{v_\phi}]$	Vector of dofs associated with the mesh on Ω_x
$\overline{\omega}$	Dimensionless load frequency	$[q^f], [q^{f_\phi}]$	Vector of dofs associated with the mesh on Ω_z
L	Length of the beam	$[q^g], [q^{g_\phi}]$	Vector of dofs associated with the mesh on ω
h	Thickness of the beam	n_x	Number of elements in the mesh on Ω_x
$S = \frac{L}{h}$	Length to thickness ratio	n_z	Number of elements in the mesh on Ω_z
		n_ω	Number of elements in the mesh on ω

The governing equations of the piezoelectric problem are given by

$$\nabla \cdot [\sigma] + [b] = \rho \frac{\partial^2 [u]}{\partial t^2} \tag{1a}$$

$$\nabla \cdot [D] - q = 0 \tag{1b}$$

where $[\sigma]$ is the stress, $[u], [D]$ are the mechanical and electric displacement respectively, $[b]$ is the prescribed body load, q is free electric volume charge and ρ is the density of the material. The two-dimensional formulation of the piezoelectric problem can be reduced to

$$\frac{\partial \sigma_{11}}{\partial x} + \frac{\partial \sigma_{13}}{\partial z} = \rho \frac{\partial^2 u_1}{\partial t^2}, \quad \frac{\partial \sigma_{13}}{\partial x} + \frac{\partial \sigma_{33}}{\partial z} = \rho \frac{\partial^2 u_3}{\partial t^2}, \quad \frac{\partial D_1}{\partial x} + \frac{\partial D_3}{\partial z} = 0 \tag{2}$$

where body load and free electric volume charge have been neglected for simplification purposes.

2.1. Constitutive relation

The constitutive equations with piezoelectric coupling for a layer k read

$$[\sigma] = \left[\overline{C}_k\right][\varepsilon] - [\bar{e}_k]^\top [E] \tag{3a}$$

$$[D] = [\bar{e}_k][\varepsilon] + [\bar{\varepsilon}_k][E] \tag{3b}$$

where $[\varepsilon] = [\varepsilon_{11}\ \varepsilon_{33}\ \gamma_{13}]^\top$ is the strain and $[E] = [E_1\ E_3]^\top$ is the electric field for the 2D formulation. Assuming plane stress in the xy-plane and also vanishing out of plane electric displacement, the reduced constitutive matrices can be computed for each layer k by

$$\left[\overline{C}_k\right] = \begin{bmatrix} C_{11}^{(k)} & C_{13}^{(k)} & 0 \\ C_{13}^{(k)} & C_{33}^{(k)} & 0 \\ 0 & 0 & C_{55}^{(k)} \end{bmatrix} - \begin{bmatrix} C_{12}^{(k)} & 0 & C_{16}^{(k)} \\ C_{23}^{(k)} & 0 & C_{36}^{(k)} \\ 0 & C_{45}^{(k)} & 0 \end{bmatrix} \begin{bmatrix} C_{22}^{(k)} & 0 & C_{26}^{(k)} \\ 0 & C_{44}^{(k)} & 0 \\ C_{26}^{(k)} & 0 & C_{66}^{(k)} \end{bmatrix}^{-1} \begin{bmatrix} C_{12}^{(k)} & C_{23}^{(k)} & 0 \\ 0 & 0 & C_{45}^{(k)} \\ C_{16}^{(k)} & C_{36}^{(k)} & 0 \end{bmatrix} \tag{4}$$

$$[\bar{e}_k] = \begin{bmatrix} 0 & 0 & e_{15}^{(k)} \\ e_{31}^{(k)} & e_{33}^{(k)} & 0 \end{bmatrix} - \begin{bmatrix} 0 & 0 & 0 \\ e_{32}^{(k)} & 0 & 0 \end{bmatrix} \begin{bmatrix} C_{22}^{(k)} & 0 & C_{26}^{(k)} \\ 0 & C_{44}^{(k)} & 0 \\ C_{26}^{(k)} & 0 & C_{66}^{(k)} \end{bmatrix}^{-1} \begin{bmatrix} C_{12}^{(k)} & C_{23}^{(k)} & 0 \\ 0 & 0 & C_{45}^{(k)} \\ C_{16}^{(k)} & C_{36}^{(k)} & 0 \end{bmatrix} \tag{5}$$

$$[\bar{\varepsilon}_k] = \begin{bmatrix} \varepsilon_{11}^{(k)} & 0 \\ 0 & \varepsilon_{33}^{(k)} \end{bmatrix} + \begin{bmatrix} 0 & 0 & 0 \\ e_{32}^{(k)} & 0 & 0 \end{bmatrix} \begin{bmatrix} C_{22}^{(k)} & 0 & C_{26}^{(k)} \\ 0 & C_{44}^{(k)} & 0 \\ C_{26}^{(k)} & 0 & C_{66}^{(k)} \end{bmatrix}^{-1} \begin{bmatrix} 0 & e_{32}^{(k)} \\ 0 & 0 \\ 0 & 0 \end{bmatrix} \tag{6}$$

being $C_{ij}^{(k)}$ the stiffness coefficients, $e_{ij}^{(k)}$ the piezoelectric constants and $\varepsilon_{ij}^{(k)}$ the permittivity coefficients for the 3D problem.

2.2. New variational formulation

For a single harmonic mechanical excitation $[F_d] = [f_d] \cdot e^{i\omega t}$ applied in $\partial_F\Omega$, the response of a linear solid in absence of body loads and free electric volume charge is presumed to have the same frequency as the applied load

$$[u(t)] = [u] \cdot e^{i\omega t}, \qquad \phi(t) = \phi \cdot e^{i\omega t} \tag{7}$$

with $[u]$ and ϕ containing the displacements and electric potential amplitudes. For a set of the load frequency within an interval $[\omega_{min}, \omega_{max}]$ a new robust variational formulation is proposed herein. The problem is defined as finding $([u(\omega)], \phi(\omega)) \in U \times \Phi$ (space of admissible generalized displacement) such that

$$\int_\omega \int_\Omega [\varepsilon(\delta u)]^\top [\sigma]\, \mathrm{d}V\, \mathrm{d}\omega - \int_\omega \int_{\partial_F\Omega} [\delta u]^\top [f_d]\, \mathrm{d}S\, \mathrm{d}\omega = \int_\omega \int_\Omega \omega^2 \rho [\delta u]^\top [u]\, \mathrm{d}V\, \mathrm{d}\omega, \tag{8a}$$

$$\int_\omega \int_\Omega [E(\delta\phi)]^\top [D]\, \mathrm{d}V\, \mathrm{d}\omega = 0, \forall ([\delta u], \delta\phi) \in \delta U \times \delta\Phi \tag{8b}$$

Using kinematic relations, $[\varepsilon] = 1/2\{\nabla[u] + \nabla[u]^\top\}$, and Maxwell's law to derive the electric field vector from the electric potential,$[E] = -\nabla\phi$, the piezoelectric problem can be reformulated only in terms of the generalized displacements $([u],\ \phi)$. To complete the boundary value problem, a prescribed displacement $[u] = [u_d]$ and electric potential $\phi = \phi_d$ are imposed on $\partial_u\Omega$ and $\partial_\phi\Omega$ respectively.

3. Separated representation

In the approach carried out in this study, the unknowns of the problem, i.e., the displacements $[u]$ and the electric potential ϕ are built under the following separated form as

$$[u] = \sum_{i=1}^{N} g^i(\omega)\left[f^i(z)\right] \circ \left[v^i(x)\right], \qquad \phi = \sum_{i=1}^{N} g_\phi^i(\omega) f_\phi^i(z)\, v_\phi^i(x) \tag{9}$$

where '$\circ$' denotes the Hadamard product. The unknown functions $\left(g^i, g_\phi^i\right)$ are defined in $[\omega_{min}, \omega_{max}]$, $\left([f^i], f_\phi^i\right)$ in Ω_z and $\left([v^i], v_\phi^i\right)$ in Ω_x. This separated representation is also used to express the virtual displacement δu and the virtual electric potential $\delta\phi$ used as test functions in Eq. (8)

$$\begin{aligned} &[\delta u] = [\delta u_\omega] + \left[\delta u_f\right] + [\delta u_v] = \delta g\,[f] \circ [v] + g \cdot [v] \circ [\delta f] + g \cdot [f] \circ [\delta v], \\ &\delta\phi = \delta\phi_\omega + \delta\phi_f + \delta\phi_v = \delta g_\phi f_\phi v_\phi + g_\phi\, \delta f_\phi\, v_\phi + g_\phi f_\phi\, \delta v_\phi \end{aligned} \tag{10}$$

The resolution process is therefore an iterative procedure where the unknown functions must be computed for each enrichment step $i = 1, 2, \ldots, n, \ldots, N$. The solution for iteration n can be expressed by

$$[u] = [\bar{u}] + g[V][f] = [\bar{u}] + g[F][v], \qquad \phi = \bar{\phi} + g_\phi f_\phi v_\phi \tag{11}$$

where $([\bar{u}], \bar{\phi})$ are the displacement and potential solution obtained at iteration $(n-1)$

$$[\bar{u}] = \sum_{i=1}^{n-1} [u^i] = \sum_{i=1}^{n-1} g^i [F^i] [v^i] = \sum_{i=1}^{n-1} g^i [V^i] [f^i], \quad \bar{\phi} = \sum_{i=1}^{n-1} \phi^i = \sum_{i=1}^{n-1} g^i_\phi f^i_\phi v^i_\phi \tag{12}$$

and

$$[v^i] = \begin{bmatrix} v^i_1(x) \\ v^i_3(x) \end{bmatrix}, \quad [V^i] = \begin{bmatrix} v^i_1(x) & 0 \\ 0 & v^i_3(x) \end{bmatrix},$$
$$[f^i] = \begin{bmatrix} f^i_1(z) \\ f^i_3(z) \end{bmatrix}, \quad [F^i] = \begin{bmatrix} f^i_1(z) & 0 \\ 0 & f^i_3(z) \end{bmatrix} \tag{13}$$

Introducing this separated representation in the piezoelectric formulation expressed by Eq. (8), the problem is decomposed into three pair coupled equations given below

$$\int_\omega \int_\Omega \left([\varepsilon(\delta u_\omega)]^\top [C] [\varepsilon(\bar{u} + g F v)] - [\varepsilon(\delta u_\omega)]^\top [e]^\top \left[E(\bar{\phi} + g_\phi f_\phi v_\phi) \right] \right) \mathrm{d}V \, \mathrm{d}\omega$$
$$- \int_\omega \int_\Omega \omega^2 \rho [\delta u_\omega]^\top [\bar{u} + g F v] \, \mathrm{d}V \, \mathrm{d}\omega = \int_\omega \int_{\partial_F \Omega} [\delta u_\omega]^\top [f_d] \, \mathrm{d}S \, \mathrm{d}\omega \tag{14a}$$

$$\int_\omega \int_\Omega \left([E(\delta\phi_\omega)]^\top [e] [\varepsilon(\bar{u} + g F v)] + [E(\delta\phi_\omega)]^\top [\varepsilon] \left[E(\bar{\phi} + g_\phi f_\phi v_\phi) \right] \right) \mathrm{d}V \, \mathrm{d}\omega = 0 \tag{14b}$$

$$\int_\omega \int_\Omega \left(\left[\varepsilon(\delta u_f) \right]^\top [C] [\varepsilon(\bar{u} + g V f)] - \left[\varepsilon(\delta u_f) \right]^\top [e]^\top \left[E(\bar{\phi} + g_\phi f_\phi v_\phi) \right] \right) \mathrm{d}V \, \mathrm{d}\omega$$
$$- \int_\omega \int_\Omega \omega^2 \rho \left[\delta u_f \right]^\top [\bar{u} + g V f] \, \mathrm{d}V \, \mathrm{d}\omega = \int_\omega \int_{\partial_F \Omega} \left[\delta u_f \right]^\top [f_d] \, \mathrm{d}S \, \mathrm{d}\omega \tag{15a}$$

$$\int_\omega \int_\Omega \left(\left[E(\delta\phi_f) \right]^\top [e] [\varepsilon(\bar{u} + g V f)] + \left[E(\delta\phi_f) \right]^\top [\varepsilon] \left[E(\bar{\phi} + g_\phi f_\phi v_\phi) \right] \right) \mathrm{d}V \, \mathrm{d}\omega = 0 \tag{15b}$$

$$\int_\omega \int_\Omega \left([\varepsilon(\delta u_v)]^\top [C] [\varepsilon(\bar{u} + g F v)] - [\varepsilon(\delta u_v)]^\top [e]^\top \left[E(\bar{\phi} + g_\phi f_\phi v_\phi) \right] \right) \mathrm{d}V \, \mathrm{d}\omega$$
$$- \int_\omega \int_\Omega \omega^2 \rho [\delta u_v]^\top [\bar{u} + g F v] \, \mathrm{d}V \, \mathrm{d}\omega = \int_\omega \int_{\partial_F \Omega} [\delta u_v]^\top [f_d] \, \mathrm{d}S \, \mathrm{d}\omega \tag{16a}$$

$$\int_\omega \int_\Omega \left([E(\delta\phi_v)]^\top [e] [\varepsilon(\bar{u} + g F v)] + [E(\delta\phi_v)]^\top [\varepsilon] \left[E(\bar{\phi} + g_\phi f_\phi v_\phi) \right] \right) \mathrm{d}V \, \mathrm{d}\omega = 0 \tag{16b}$$

These three pairs coupled equations define a non-linear problem. To solve it, an iterative procedure is followed. The fixed point loop is iterated m times until reaching a fixed solution for each enrichment step n which composes the final solution. This resolution strategy is explained in Algorithm 1.

Algorithm 1: Fixed point loop applied to the piezoelectric problem.

for $n = 1$ to N **do**
  Initialize $\left(g, g_\phi\right)^0$, $\left([f], f_\phi\right)^{(0)}$ and compute $\left([v], v_\phi\right)^{(0)}$ from Eq. (16)
  for $m = 1$ to m_{max} **do**
    Step 1: knowing $\left([v], v_\phi\right)^{(m-1)}$, $\left([f], f_\phi\right)^{(m-1)}$, compute $\left(g, g_\phi\right)^{(m)}$ from Eq. (14)
    Step 2: knowing $\left([v], v_\phi\right)^{(m-1)}$, $\left(g, g_\phi\right)^{(m)}$, compute $\left([f], f_\phi\right)^{(m)}$ from Eq. (15)
    Step 3: knowing $\left([f], f_\phi\right)^{(m)}$, $\left(g, g_\phi\right)^{(m)}$, compute $\left([v], v_\phi\right)^{(m)}$ from Eq. (16)
    Check for convergence (break)
  end for
  Set $g^n = g^{(m)}, [f^n] = [f]^{(m)}, [v^n] = [v]^{(m)}$ and $g^n_\phi = g^{(m)}_\phi, f^n_\phi = f^{(m)}_\phi, v^n_\phi = v^{(m)}_\phi$
  Set $[u^n] = \left[u^{n-1}\right] + g^n [V^n] [f^n]$ and $\phi^n = \phi^{n-1} + g^n_\phi f^n_\phi v^n_\phi$
end for

3.1. Step 1: Problem on load frequency domain

In order to simplify the notation, the functions $\left([f], f_\phi\right)^{(m-1)}, \left([v], v_\phi\right)^{(m-1)}$, which are assumed to be known, will be denoted as $\tilde{f}, \tilde{f}_\phi, \tilde{v}, \tilde{v}_\phi$ (and subsequently $\tilde{F}, \tilde{V}$ in matrix form) and the functions $g^{(m)}, g^{(m)}_\phi$ to be computed will be denoted as g, g_ϕ. The strain and electric fields are defined in matrix notation as

$$\left[\varepsilon\left(g \tilde{F} \tilde{v}\right)\right] = g \left[\Sigma_z\left(\tilde{f}\right)\right] \left[\mathscr{E}_v\right], \qquad \left[E\left(g_\phi \tilde{f}_\phi \tilde{v}_\phi\right)\right] = g_\phi \left[\Sigma^\phi_z\left(\tilde{f}_\phi\right)\right] \left[\mathscr{E}_{v_\phi}\right] \tag{17}$$

with

$$\left[\Sigma_z\left(\tilde{f}\right)\right] = \begin{bmatrix} 0 & \tilde{f}_1 & 0 & 0 \\ 0 & 0 & \tilde{f}'_3 & 0 \\ \tilde{f}'_1 & 0 & 0 & \tilde{f}_3 \end{bmatrix}, \left[\mathscr{E}_v\right] = \left[v_1 \; v'_1 \; v_3 \; v'_3\right]^\top,$$
$$\left[\Sigma^\phi_z\left(\tilde{f}_\phi\right)\right] = \begin{bmatrix} 0 & -\tilde{f}_\phi \\ -\tilde{f}'_\phi & 0 \end{bmatrix}, \left[\mathscr{E}_{v_\phi}\right] = \left[v_\phi \; v'_\phi\right]^\top \tag{18}$$

where the prime ($'$) stands for the classical derivation. Introducing the above expression into Eq. (14), the variational problem defined on load frequency domain read

$$\int_\omega \delta g \, k^{vv}_\omega \, g \, \mathrm{d}\omega - \int_\omega \delta g \, k^{v\phi}_\omega \, g_\phi \, \mathrm{d}\omega - \int_\omega \delta g \, \omega^2 m_\omega \, g \, \mathrm{d}\omega$$
$$= \int_\omega \delta g f_\omega \, \mathrm{d}\omega + \sum_{i=1}^{n-1} \left[\int_\omega \delta g \, \omega^2 \mu^i_\omega \bar{g}^i \, \mathrm{d}\omega - \int_\omega \delta g \, \sigma^{vv^i}_\omega \bar{g}^i \, \mathrm{d}\omega + \int_\omega \delta g \, \sigma^{v\phi^i}_\omega \bar{g}^i_\phi \, \mathrm{d}\omega \right] \tag{19a}$$

$$- \int_\omega \delta g_\phi \, k^{\phi v}_\omega \, g \, \mathrm{d}\omega - \int_\omega \delta g_\phi \, k^{\phi\phi}_\omega \, g_\phi \, \mathrm{d}\omega \sum_{i=1}^{n-1} \left[\int_\omega \delta g_\phi \, \sigma^{\phi v^i}_\omega \bar{g}^i \, \mathrm{d}\omega + \int_\omega \delta g_\phi \, \sigma^{\phi\phi^i}_\omega \bar{g}^i_\phi \, \mathrm{d}\omega \right] \tag{19b}$$

where the functions with the superscript "i" are referred to the solution at the previous enrichment steps $i = 1, 2, \ldots, (n-1)$. The coefficients integrated in the spatial domain Ω are

$$
\begin{aligned}
&k_\omega^{vv}\left(\tilde{f},\tilde{v}\right)=\int_\Omega\left[\tilde{\mathscr{E}}_v\right]^\top[\tilde{\Sigma}_z]^\top[C][\tilde{\Sigma}_z]\left[\tilde{\mathscr{E}}_v\right]\mathrm{d}V, && k_\omega^{v\phi}\left(\tilde{f},\tilde{f}_\phi,\tilde{v},\tilde{v}_\phi\right)=\int_\Omega\left[\tilde{\mathscr{E}}_v\right]^\top[\tilde{\Sigma}_z]^\top[e]^\top[\tilde{\Sigma}_z^\phi]\left[\tilde{\mathscr{E}}_{v_\phi}\right]\mathrm{d}V,\\
&k_\omega^{\phi v}\left(\tilde{f},\tilde{f}_\phi,\tilde{v},\tilde{v}_\phi\right)=\int_\Omega\left[\tilde{\mathscr{E}}_{v_\phi}\right]^\top[\tilde{\Sigma}_z^\phi]^\top[e][\tilde{\Sigma}_z]\left[\tilde{\mathscr{E}}_v\right]\mathrm{d}V, && k_\omega^{\phi\phi}\left(\tilde{f}_\phi,\tilde{v}_\phi\right)=\int_\Omega\left[\tilde{\mathscr{E}}_{v_\phi}\right]^\top[\tilde{\Sigma}_z^\phi]^\top[\epsilon][\tilde{\Sigma}_z^\phi]\left[\tilde{\mathscr{E}}_{v_\phi}\right]\mathrm{d}V,\\
&\sigma_\omega^{vv^i}\left(\tilde{f},\tilde{v},\bar{f}^i,\bar{v}^i\right)=\int_\Omega\left[\tilde{\mathscr{E}}_v\right]^\top[\tilde{\Sigma}_z]^\top[C][\bar{\Sigma}_z^i]\left[\bar{\mathscr{E}}_v^i\right]\mathrm{d}V, && \sigma_\omega^{v\phi^i}\left(\tilde{f},\tilde{v},\bar{f}_\phi^i,\bar{v}_\phi^i\right)=\int_\Omega\left[\tilde{\mathscr{E}}_v\right]^\top[\tilde{\Sigma}_z]^\top[e]^\top\left[\bar{\Sigma}_z^{\phi^i}\right]\left[\bar{\mathscr{E}}_{v_\phi}^i\right]\mathrm{d}V,\\
&\sigma_\omega^{\phi v^i}\left(\tilde{f}_\phi,\tilde{v}_\phi,\bar{f}^i,\bar{v}^i\right)=\int_\Omega\left[\tilde{\mathscr{E}}_{v_\phi}\right]^\top[\tilde{\Sigma}_z^\phi]^\top[e][\bar{\Sigma}_z^i]\left[\bar{\mathscr{E}}_v^i\right]\mathrm{d}V, && \sigma_\omega^{\phi\phi^i}\left(\tilde{f}_\phi,\tilde{v}_\phi,\bar{f}_\phi^i,\bar{v}_\phi^i\right)=\int_\Omega\left[\tilde{\mathscr{E}}_{v_\phi}\right]^\top[\tilde{\Sigma}_z^\phi]^\top[\epsilon]\left[\bar{\Sigma}_z^{\phi^i}\right]\left[\bar{\mathscr{E}}_{v_\phi}^i\right]\mathrm{d}V,\\
&m_\omega\left(\tilde{f},\tilde{v}\right)=\int_\Omega[\tilde{v}]^\top\left[\tilde{F}\right]^\top\rho\left[\tilde{F}\right][\tilde{v}]\,\mathrm{d}V, && \mu_\omega^i\left(\tilde{f},\bar{f}^i,\bar{v}^i\right)=\int_\Omega[\tilde{v}]^\top\left[\tilde{F}\right]^\top\rho\left[\bar{F}^i\right][\bar{v}^i]\,\mathrm{d}V,\\
&f_\omega\left(\tilde{f},\tilde{v}\right)=\int_{\partial_F\Omega}[\tilde{v}]^\top\left[\tilde{F}\right]^\top[f_d]\,\mathrm{d}S
\end{aligned}
\tag{20}
$$

Note that for any particular value of the pulsation ω, it is easy to notice that the Eq. (19) results in

$$
\left(k_\omega^{vv}-\omega^2 m_\omega\right)g-k_\omega^{v\phi}g_\phi=f_\omega+\sum_{i=1}^{n-1}[\ldots] \tag{21a}
$$

$$
-k_\omega^{\phi v}g-k_\omega^{\phi\phi}g_\phi=\sum_{i=1}^{n-1}[\ldots] \tag{21b}
$$

These two equations can be combined in order to find an explicit expression for g such that

$$
\left[k_\omega^{\phi\phi}\left(k_\omega^{vv}-\omega^2 m_\omega\right)+k_\omega^{\phi v}k_\omega^{v\phi}\right]g=f_\omega+\sum_{i=1}^{n-1}[\ldots] \tag{22}
$$

from which we can derive the value of the natural frequencies, ω_n, for which the resonance is detected

$$
\omega_n^2=\frac{k_\omega^{vv}+\left(k_\omega^{v\phi}\right)^2/k_\omega^{\phi\phi}}{m_\omega} \tag{23}
$$

3.2. Step 2: Problem on Ω_z

At this step, the functions $(g,g_\phi)^{(m)}$, $([v],v_\phi)^{(m-1)}$, assumed to be known, will be denoted as $\tilde{g},\tilde{g}_\phi,\tilde{v},\tilde{v}_\phi$ and the functions $([f],f_\phi)^{(m)}$ to be computed will be denoted as f,f_ϕ. The strain and electric field are defined in matrix notation as

$$
\left[\varepsilon\left(\tilde{g}\;\tilde{V}\,f\right)\right]=\tilde{g}\left[\Sigma_x(\tilde{v})\right]\left[\mathscr{E}_f\right],\qquad\left[E\left(\tilde{g}_\phi\,\tilde{v}_\phi f_\phi\right)\right]=\tilde{g}_\phi\left[\Sigma_x^\phi(\tilde{v}_\phi)\right]\left[\mathscr{E}_{f_\phi}\right], \tag{24}
$$

with

$$
\begin{aligned}
&\left[\Sigma_x(\tilde{v})\right]=\begin{bmatrix}\tilde{v}_1' & 0 & 0 & 0\\ 0 & 0 & 0 & \tilde{v}_3\\ 0 & \tilde{v}_1 & \tilde{v}_3' & 0\end{bmatrix},\ \left[\mathscr{E}_f\right]=\left[f_1\,f_1'\,f_3\,f_3'\right]^\top,\\
&\left[\Sigma_x^\phi(\tilde{v}_\phi)\right]=\begin{bmatrix}-\tilde{v}_\phi' & 0\\ 0 & -\tilde{v}_\phi\end{bmatrix},\ \left[\mathscr{E}_{f_\phi}\right]=\left[f_\phi\,f_\phi'\right]^\top
\end{aligned}
\tag{25}
$$

Introducing the above expression into Eq. (15), the variational problem defined on Ω_z is

$$
\begin{aligned}
&\gamma_\omega\int_{\Omega_z}[\delta\mathscr{E}_f]^\top\left[k_x^{ff}\right][\mathscr{E}_f]\,\mathrm{d}z-\theta_\omega\int_{\Omega_z}[\delta\mathscr{E}_f]^\top\left[k_x^{f\phi}\right]\left[\mathscr{E}_{f_\phi}\right]\mathrm{d}z-\alpha_\omega\int_{\Omega_z}[\delta f]^\top[m_x][f]\,\mathrm{d}z\\
&=\beta_\omega\int_{\partial_F\Omega_z}[\delta f]^\top[f_x]\,\mathrm{d}z+\sum_{i=1}^{n-1}\left[\alpha_\omega^i\int_{\Omega_z}[\delta f]^\top[\mu_x^i]\left[\bar{f}^i\right]\mathrm{d}z-\gamma_\omega^i\int_{\Omega_z}[\delta\mathscr{E}_f]^\top\left[\sigma_x^{ff^i}\right]\left[\bar{\mathscr{E}}_f^i\right]\mathrm{d}z\right.\\
&\quad\left.+\theta_\omega^{g\phi^i}\int_{\Omega_z}[\delta\mathscr{E}_f]^\top\left[\sigma_x^{f\phi^i}\right]\left[\bar{\mathscr{E}}_{f_\phi}^i\right]\mathrm{d}z\right]
\end{aligned}
\tag{26a}
$$

$$
\begin{aligned}
&-\theta_\omega\int_{\Omega_z}\left[\delta\mathscr{E}_{f_\phi}\right]^\top\left[k_x^{\phi f}\right][\mathscr{E}_f]\,\mathrm{d}z-\eta_\omega\int_{\Omega_z}\left[\delta\mathscr{E}_{f_\phi}\right]^\top\left[k_x^{\phi\phi}\right]\left[\mathscr{E}_{f_\phi}\right]\mathrm{d}z\\
&=\sum_{i=1}^{n-1}\left[\theta_\omega^{\phi g^i}\int_{\Omega_z}\left[\delta\mathscr{E}_{f_\phi}\right]^\top\left[\sigma_x^{\phi f^i}\right]\left[\bar{\mathscr{E}}_f^i\right]\mathrm{d}z+\eta_\omega^i\int_{\Omega_z}\left[\delta\mathscr{E}_{f_\phi}\right]^\top\left[\sigma_x^{\phi\phi^i}\right]\left[\bar{\mathscr{E}}_{f_\phi}^i\right]\mathrm{d}z\right]
\end{aligned}
\tag{26b}
$$

where the coefficients integrated in the Ω_x domain are

$$
\begin{aligned}
&\left[k_x^{ff}(\tilde{v})\right]=\int_{\Omega_x}[\tilde{\Sigma}_x]^\top[C][\tilde{\Sigma}_x]\,\mathrm{d}x, && \left[k_x^{f\phi}\left(\tilde{v},\tilde{v}_\phi\right)\right]=\int_{\Omega_x}[\tilde{\Sigma}_x]^\top[e]^\top[\tilde{\Sigma}_x^\phi]\,\mathrm{d}x,\\
&\left[k_x^{\phi f}\left(\tilde{v},\tilde{v}_\phi\right)\right]=\int_{\Omega_x}[\tilde{\Sigma}_x^\phi]^\top[e][\tilde{\Sigma}_x]\,\mathrm{d}x, && \left[k_x^{\phi\phi}\left(\tilde{v}_\phi\right)\right]=\int_{\Omega_x}[\tilde{\Sigma}_x^\phi]^\top[\epsilon][\tilde{\Sigma}_x^\phi]\,\mathrm{d}x,\\
&\left[\sigma_x^{ff^i}(\tilde{v},\bar{v}^i)\right]=\int_{\Omega_x}[\tilde{\Sigma}_x]^\top[C][\bar{\Sigma}_x^i]\,\mathrm{d}x, && \left[\sigma_x^{f\phi^i}\left(\tilde{v},\bar{v}_\phi^i\right)\right]=\int_{\Omega_x}[\tilde{\Sigma}_x]^\top[e]^\top\left[\bar{\Sigma}_x^{\phi^i}\right]\mathrm{d}x,\\
&\left[\sigma_x^{\phi f^i}(\tilde{v}_\phi,\bar{v}^i)\right]=\int_{\Omega_x}[\tilde{\Sigma}_x^\phi]^\top[e][\bar{\Sigma}_x^i]\,\mathrm{d}x, && \left[\sigma_x^{\phi\phi^i}\left(\tilde{v}_\phi,\bar{v}_\phi^i\right)\right]=\int_{\Omega_x}[\tilde{\Sigma}_x^\phi]^\top[\epsilon]\left[\bar{\Sigma}_x^{\phi^i}\right]\mathrm{d}x,\\
&[m_x(\tilde{v})]=\int_{\Omega_x}\left[\tilde{V}\right]^\top\rho\left[\tilde{V}\right]\mathrm{d}x, && \left[\mu_x^i(\tilde{v},\bar{v}^i)\right]=\int_{\Omega_x}\left[\tilde{V}\right]^\top\rho\left[\bar{V}^i\right]\mathrm{d}x,\\
&[f_x(\tilde{v})]=\int_{\partial_F\Omega_x}\left[\tilde{V}\right]^\top[f_d]\,\mathrm{d}x
\end{aligned}
\tag{27}
$$

and the coefficients integrated in the load frequency domain are

$$
\begin{aligned}
&\gamma_\omega(\tilde{g})=\int_\omega\tilde{g}^2\,\mathrm{d}\omega, && \gamma_\omega^i(\tilde{g},\bar{g}^i)=\int_\omega\tilde{g}\bar{g}^i\,\mathrm{d}\omega,\\
&\eta_\omega(\tilde{g},\tilde{g}_\phi)=\int_\omega\tilde{g}\tilde{g}_\phi\,\mathrm{d}\omega, && \eta_\omega(\tilde{g}_\phi)=\int_\omega\tilde{g}_\phi^2\,\mathrm{d}\omega,\\
&\alpha_\omega(\tilde{g})=\int_\omega\omega^2\tilde{g}^2\,\mathrm{d}\omega, && \alpha_\omega^i(\tilde{g},\bar{g}^i)=\int_\omega\omega^2\tilde{g}\bar{g}^i\,\mathrm{d}\omega,\\
&\beta_\omega(\tilde{g})=\int_\omega\tilde{g}\,\mathrm{d}\omega, && \theta_\omega(\tilde{g},\tilde{g}_\phi)=\int_\omega\tilde{g}\tilde{g}_\phi\,\mathrm{d}\omega\\
&\theta_\omega^{g\phi^i}(\tilde{g},\bar{g}_\phi^i)=\int_\omega\tilde{g}\bar{g}_\phi^i\,\mathrm{d}\omega, && \theta_\omega^{\phi g^i}(\tilde{g}_\phi,\bar{g}^i)=\int_\omega\tilde{g}_\phi\bar{g}^i\,\mathrm{d}\omega
\end{aligned}
\tag{28}
$$

3.3. Step 3: Problem on Ω_x

At this step, the functions $(g,g_\phi)^{(m)}$, $([f],f_\phi)^{(m)}$, which are assumed to be known, will be denoted as $\tilde{g},\tilde{g}_\phi,\tilde{f},\tilde{f}_\phi$ and the functions $([v],v_\phi)^{(m)}$ to be computed will be denoted as v,v_ϕ. The expression of the strain and electric field are

$$
\left[\varepsilon\left(\tilde{g}\;\tilde{F}\;v\right)\right]=\tilde{g}\left[\Sigma_z\left(\tilde{f}\right)\right][\mathscr{E}_v],\quad\left[E\left(\tilde{g}_\phi\tilde{f}_\phi\,v_\phi\right)\right]=\tilde{g}_\phi\left[\Sigma_z^\phi\left(\tilde{f}_\phi\right)\right]\left[\mathscr{E}_{v_\phi}\right] \tag{29}
$$

Introducing the above expression into Eq. (16), the variational problem defined on Ω_x read

$$
\begin{aligned}
&\gamma_\omega\int_{\Omega_x}[\delta\mathscr{E}_v]^\top\left[k_z^{vv}\right][\mathscr{E}_v]\,\mathrm{d}x-\theta_\omega\int_{\Omega_x}[\delta\mathscr{E}_v]^\top\left[k_z^{v\phi}\right]\left[\mathscr{E}_{v_\phi}\right]\mathrm{d}x-\alpha_\omega\int_{\Omega_x}[\delta v]^\top[m_z][v]\,\mathrm{d}x\\
&=\beta_\omega\int_{\partial_F\Omega_x}[\delta v]^\top[f_z]\,\mathrm{d}x+\sum_{i=1}^{n-1}\left[\alpha_\omega^i\int_{\Omega_x}[\delta v]^\top\left[\mu_z^i\right]\left[\bar{v}^i\right]\mathrm{d}x\right.\\
&\quad\left.-\gamma_\omega^i\int_{\Omega_x}[\delta\mathscr{E}_v]^\top\left[\sigma_z^{vv^i}\right]\left[\bar{\mathscr{E}}_v^i\right]\mathrm{d}x+\theta_\omega^{g\phi^i}\int_{\Omega_x}[\delta\mathscr{E}_v]^\top\left[\sigma_z^{v\phi^i}\right]\left[\bar{\mathscr{E}}_{v_\phi}^i\right]\mathrm{d}x\right]
\end{aligned}
\tag{30a}
$$

$$
\begin{aligned}
&-\theta_\omega \int_{\Omega_x} \left[\delta\mathscr{E}_{v_\phi}\right]^\top \left[k_z^{\phi v}\right] \left[\mathscr{E}_v\right] x - \eta_\omega \int_{\Omega_x} \left[\delta\mathscr{E}_{v_\phi}\right]^\top \left[k_z^{\phi\phi}\right] \left[\mathscr{E}_{v_\phi}\right] \mathrm{d}x \\
&= \sum_{i=1}^{n-1} \left[\theta_\omega^{\phi g^i} \int_{\Omega_x} \left[\delta\mathscr{E}_{v_\phi}\right]^\top \left[\sigma_z^{\phi v^i}\right] \left[\bar{\mathscr{E}}_v^i\right] \mathrm{d}x + \eta_\omega^i \int_{\Omega_x} \left[\delta\mathscr{E}_{v_\phi}\right]^\top \left[\sigma_z^{\phi\phi^i}\right] \left[\bar{\mathscr{E}}_{v_\phi}^i\right] \mathrm{d}x \right]
\end{aligned} \tag{30b}
$$

where the coefficients integrated in the Ω_z domain are

$$
\begin{aligned}
&\left[k_z^{vv}\left(\tilde{f}\right)\right] = \int_{\Omega_z} \left[\tilde{\Sigma}_z\right]^\top [C] \left[\tilde{\Sigma}_z\right] \mathrm{d}z, && \left[k_z^{v\phi}\left(\tilde{f},\tilde{f}_\phi\right)\right] = \int_{\Omega_z} \left[\tilde{\Sigma}_z\right]^\top [e]^\top \left[\tilde{\Sigma}_z^\phi\right] \mathrm{d}z, \\
&\left[k_z^{\phi v}\left(\tilde{f},\tilde{f}_\phi\right)\right] = \int_{\Omega_z} \left[\tilde{\Sigma}_z^\phi\right]^\top [e] \left[\tilde{\Sigma}_z\right] \mathrm{d}z, && \left[k_z^{\phi\phi}\left(\tilde{f}_\phi\right)\right] = \int_{\Omega_z} \left[\tilde{\Sigma}_z^\phi\right]^\top [\varepsilon] \left[\tilde{\Sigma}_z^\phi\right] \mathrm{d}z, \\
&\left[\sigma_z^{vv^i}\left(\tilde{f},\bar{f}^i\right)\right] = \int_{\Omega_z} \left[\tilde{\Sigma}_z\right]^\top [C] \left[\bar{\Sigma}_z^i\right] \mathrm{d}z, && \left[\sigma_z^{v\phi^i}\left(\tilde{f},\bar{f}_\phi^i\right)\right] = \int_{\Omega_z} \left[\tilde{\Sigma}_z\right]^\top [e]^\top \left[\bar{\Sigma}_z^{\phi^i}\right] \mathrm{d}z, \\
&\left[\sigma_z^{\phi v^i}\left(\tilde{f}_\phi,\bar{f}^i\right)\right] = \int_{\Omega_z} \left[\tilde{\Sigma}_z^\phi\right]^\top [e] \left[\bar{\Sigma}_z^i\right] \mathrm{d}z, && \left[\sigma_z^{\phi\phi^i}\left(\tilde{f}_\phi,\bar{f}_\phi^i\right)\right] = \int_{\Omega_z} \left[\tilde{\Sigma}_z^\phi\right]^\top [\varepsilon] \left[\bar{\Sigma}_z^{\phi^i}\right] \mathrm{d}z, \\
&\left[m_z\left(\tilde{f}\right)\right] = \int_{\Omega_z} \left[\tilde{F}\right]^\top \rho \left[\tilde{F}\right] \mathrm{d}z, && \left[\mu_z^i\left(\tilde{f},\bar{f}^i\right)\right] = \int_{\Omega_z} \left[\tilde{F}\right]^\top \rho \left[\bar{F}^i\right] \mathrm{d}z, \\
&\left[f_z\left(\tilde{f}\right)\right] = \int_{\partial_F\Omega_z} \left[\tilde{F}\right]^\top [f_d] \mathrm{d}z
\end{aligned} \tag{31}
$$

and the ones integrated in the load frequency domain are expressed by Eq. 28.

4. FE discretization

To numerically compute the solution, a discrete representation of the unknown functions is addressed. For the load frequency domain, a uniform discretization of the interval $[\omega_{min}, \omega_{max}]$ is set up. The elementary vectors of degrees of freedoms (dofs) associated with the mesh in ω are $\left[q_h^g\right], \left[q_h^{g_\phi}\right]$. On the other hand, a classical finite element approximation is used in domains Ω_x and Ω_z. The elementary vectors of dofs associated with the mesh in Ω_x and Ω_z are $\left[q_e^v\right], \left[q_e^{v_\phi}\right]$ and $\left[q_k^f\right], \left[q_k^{f_\phi}\right]$ respectively. Under these assumptions, unknown functions and derived fields are approximated as follows

$$
[v_e] = [N_x]\left[q_e^v\right], \quad \left[\mathscr{E}_v^e\right] = [B_x]\left[q_e^v\right], \quad \left[v_{\phi_e}\right] = \left[N_{\phi x}\right]\left[q_e^{v_\phi}\right], \quad \left[E_{v_\phi}^e\right] = \left[B_{\phi x}\right]\left[q_e^{v_\phi}\right] \tag{32}
$$

$$
[f_k] = [N_z]\left[q_k^f\right], \quad \left[\mathscr{E}_f^k\right] = [B_z]\left[q_k^f\right], \quad \left[f_{\phi_k}\right] = \left[N_{\phi z}\right]\left[q_k^{f_\phi}\right], \quad \left[E_{f_\phi}^k\right] = \left[B_{\phi z}\right]\left[q_k^{f_\phi}\right] \tag{33}
$$

$$
[g_h] = [N_\omega]\left[q_h^g\right], \quad \left[g_{\phi_h}\right] = \left[N_{\phi\omega}\right]\left[q_h^{g_\phi}\right] \tag{34}
$$

where the matrices $[N_x], \left[N_{\phi x}\right], [B_x]$ and $\left[B_{\phi x}\right]$ contain the shape functions and their derivatives for the problem on Ω_x and analogously for the other domains. The total number of elements in $[\omega_{min}, \omega_{max}] = \bigcup_{h=1}^{n_\omega} \omega^h, \Omega_x = \bigcup_{e=1}^{n_x} \Omega_x^e$ and $\Omega_z = \bigcup_{k=1}^{n_z} \Omega_z^k$ domains are denoted as n_ω, n_x and n_z, respectively. Note that the interpolation can be different for each domain and also for the mechanical and electric unknowns separately. The introduction of the discretization in Eq. (30b) lead to the electro-mechanical linear system

Problem on Ω_x :

$$
\left(\begin{bmatrix} [K_{vv}] & -\left[K_{vv_\phi}\right] \\ -\left[K_{vv_\phi}\right]^\top & -\left[K_{v_\phi v_\phi}\right] \end{bmatrix} - \begin{bmatrix} [M_v] & [\bar{0}] \\ [\bar{0}] & [\bar{0}] \end{bmatrix} \right) \begin{bmatrix} [q^v] \\ [q^{v_\phi}] \end{bmatrix} = \begin{bmatrix} [F_v] + [R_f] \\ [R_{v_\phi}] \end{bmatrix} \tag{35}
$$

where

- $[q^v], [q^{v_\phi}]$ are the vector of dofs associated with the finite element mesh in Ω_x for the mechanical and electric unknowns respectively.
- $[K_{vv}], \left[K_{vv_\phi}\right], \left[K_{v_\phi v_\phi}\right]$ are the stiffness, electro-mechanical and dielectric matrices obtained by assembling the elementary matrices $\left[K_{vv}^e\right], \left[K_{vv_\phi}^e\right], \left[K_{v_\phi v_\phi}^e\right]$, respectively

$$
\left[K_{vv}^e\left(\tilde{g},\tilde{f}\right)\right] = \left[\sum_{h=1}^{n_\omega} \gamma_\omega(\tilde{g}_h)\right] \int_{\Omega_x^e} [B_x]^\top \left[\sum_{k=1}^{n_z} \left[k_z^{vv}\left(\tilde{f}_k\right)\right]\right] [B_x] \mathrm{d}x \tag{36}
$$

$$
\left[K_{vv_\phi}^e\left(\tilde{g},\tilde{g}_\phi,\tilde{f},\tilde{f}_\phi\right)\right] = \left[\sum_{h=1}^{n_\omega} \theta_\omega(\tilde{g}_h,\tilde{g}_{\phi h})\right] \int_{\Omega_x^e} [B_x]^\top \left[\sum_{k=1}^{n_z} \left[k_z^{v\phi}\left(\tilde{f}_k,\tilde{f}_{\phi_k}\right)\right]\right] \left[B_{\phi x}\right] \mathrm{d}x \tag{37}
$$

$$
\left[K_{v_\phi v_\phi}^e\left(\tilde{g}_\phi,\tilde{f}_\phi\right)\right] = \left[\sum_{h=1}^{n_\omega} \eta_\omega(\tilde{g}_{\phi_h})\right] \int_{\Omega_x^e} \left[B_{\phi x}\right]^\top \left[\sum_{k=1}^{n_z} \left[k_z^{\phi\phi}\left(\tilde{f}_{\phi_k}\right)\right]\right] \left[B_{\phi x}\right] \mathrm{d}x \tag{38}
$$

- $[M_v]$ is the mass matrix obtained by assembling the elementary mass matrices $\left[M_v^e\right]$

$$
\left[M_v^e\left(\tilde{g},\tilde{f}\right)\right] = \left[\sum_{h=1}^{n_\omega} \alpha_\omega(\tilde{g}_h)\right] \int_{\Omega_x^e} [N_x]^\top \left[\sum_{k=1}^{n_z} \left[m_z\left(\tilde{f}_k\right)\right]\right] [N_x] \mathrm{d}x \tag{39}
$$

- $[F_v]$ is the load vector obtained by assembling the elementary load vectors $\left[F_v^e\right]$

$$
\left[F_v^e\left(\tilde{g},\tilde{f}\right)\right] = \left[\sum_{h=1}^{n_\omega} \beta_\omega(\tilde{g}_h)\right] \int_{\partial_F\Omega_x^e} [N_x]^\top \left[\sum_{k=1}^{n_z} \left[f_z\left(\tilde{f}_k\right)\right]\right] \mathrm{d}x \tag{40}
$$

- $[R_v], \left[R_{v_\phi}\right]$ are the equilibrium residuals, obtained by assembling the elementary residual vectors $\left[R_v^e\right], \left[R_{v_\phi}^e\right]$

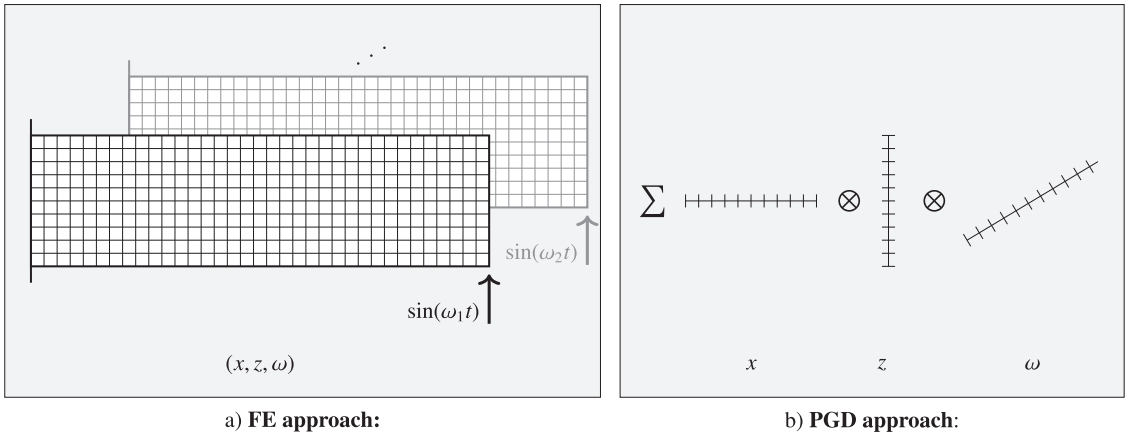

a) **FE approach:**

n_ω resolutions of a 2D problem with $n_x \times n_z$ elements

problem size $\sim (n_\omega \times n_x \times n_z)$

b) **PGD approach**:

N iterations of three 1D problems of n_ω, n_x and n_z elements

problem size $\sim N \times (n_\omega + n_x + n_z)$

Fig. 2. Diagram of the new PGD formulation and comparison with the classical 2D layerwise FE approach.

$$\left[R_v^e\left(\tilde{g},\tilde{f},\bar{u},\bar{\phi}\right)\right] = \sum_{i=1}^{n-1}\left\{\left[\sum_{h=1}^{n_\omega}\alpha_\omega^i\left(\tilde{g}_h,\bar{g}_h^i\right)\right]\int_{\Omega_x^e}[N_x]^\top\left[\sum_{k=1}^{n_z}\left[\mu_z^i\left(\tilde{f}_k,\bar{f}_k^i\right)\right]\right][\bar{v}^i]\,\mathrm{d}x\right.$$
$$-\left[\sum_{h=1}^{n_\omega}\gamma_\omega^i\left(\tilde{g}_h,\bar{g}_h^i\right)\right]\int_{\Omega_x^e}[B_x]^\top\left[\sum_{k=1}^{n_z}\left[\sigma_z^{v v^i}\left(\tilde{f}_k,\bar{f}_k^i\right)\right]\right][\bar{\delta}_v^i]\,\mathrm{d}x$$
$$\left.+\left[\sum_{h=1}^{n_\omega}\theta_\omega^{g\phi^i}\left(\tilde{g}_h,\bar{g}_{\phi_h}^i\right)\right]\int_{\Omega_x^e}[B_x]^\top\left[\sum_{k=1}^{n_z}\left[\sigma_z^{v\phi^i}\left(\tilde{f}_k,\bar{f}_{\phi_k}^i\right)\right]\right][\bar{\delta}_{v_\phi}^i]\,\mathrm{d}x\right\} \tag{41}$$

$$\left[R_{v_\phi}^e\left(\tilde{g}_\phi,\tilde{f}_\phi,\bar{u},\bar{\phi}\right)\right] = \sum_{i=1}^{n-1}\left\{\left[\sum_{h=1}^{n_\omega}\theta_\omega^{\phi g^i}\left(\tilde{g}_{\phi_h},\bar{g}_h^i\right)\right]\int_{\Omega_x^e}[B_{\phi x}]^\top\left[\sum_{k=1}^{n_z}\left[\sigma_z^{\phi v^i}\left(\tilde{f}_{\phi_k},\bar{f}_k^i\right)\right]\right][\bar{\delta}_v^i]\,\mathrm{d}x\right.$$
$$\left.+\left[\sum_{h=1}^{n_\omega}\eta_\omega^i\left(\tilde{g}_{\phi_h},\bar{g}_{\phi_h}^i\right)\right]\int_{\Omega_x^e}[B_{\phi x}]^\top\left[\sum_{k=1}^{n_z}\left[\sigma_z^{\phi\phi^i}\left(\tilde{f}_{\phi_k},\bar{f}_{\phi_k}^i\right)\right]\right][\bar{\delta}_{v_\phi}^i]\,\mathrm{d}x\right\} \tag{42}$$

Analogously, the introduction of the discretization in the Eqs. (26) and (19) lead to the next electro-mechanical linear systems

Problem on Ω_z :

$$\left(\begin{bmatrix}[K_{ff}] & -[K_{ff_\phi}]\\ -[K_{ff_\phi}]^\top & -[K_{f_\phi f_\phi}]\end{bmatrix} - \begin{bmatrix}[M_f] & [\bar{0}]\\ [\bar{0}] & [\bar{0}]\end{bmatrix}\right)\begin{bmatrix}[q^f]\\ [q^{f_\phi}]\end{bmatrix} = \begin{bmatrix}[F_f]+[R_f]\\ [R_{f_\phi}]\end{bmatrix} \tag{43}$$

Problem on ω :

$$\left(\begin{bmatrix}[K_{gg}] & -[K_{gg_\phi}]\\ -[K_{gg_\phi}]^\top & -[K_{g_\phi g_\phi}]\end{bmatrix} - \begin{bmatrix}[M_g] & [\bar{0}]\\ [\bar{0}] & [\bar{0}]\end{bmatrix}\right)\begin{bmatrix}[q^g]\\ [q^{g_\phi}]\end{bmatrix} = \begin{bmatrix}[F_g]+[R_g]\\ [R_{g_\phi}]\end{bmatrix} \tag{44}$$

where the components have a similar formulation and interpretation to that already presented for the problem on Ω_x domain. The separated representation and reduction in the degrees of freedom to which the PGD leads is depicted in the diagram of Fig. 2.

5. Numerical tests

This section is dedicated to the dynamic analysis of some piezoelectric composite beams in order to evaluate the proposed methodology. It should be mentioned that the PGD method has been successfully used to the harmonic analysis of composite beams [49] but also to solve static problems of piezoelectric plates [50]. This paper aims to extend the PGD formulation to the harmonic analysis of piezoelectric composite beams in the frequency domain. The Frequency Response Functions (FRF) are obtained for the first time by using the PGD method for the piezoelectric problem. In addition, the proposed formulation allows us to identify the modal parameters, natural frequencies and vibration modes, for both short circuit and open circuit conditions. In the following numerical test cases, the proposed approach will be evaluated by first addressing the eigenfrequencies and eigenmodes and subsequently the FRF.

In these tests, as far as the spatial discretization is concerned, a classical quadratic finite element approximation is considered for both domains Ω_x and Ω_z. A Gaussian numerical integration with three points is used to evaluate the elementary matrices and also to compute the integrals in the load frequency domain. The results are compared with classical finite element solutions and exact elastic solutions or models available in the literature. The software ANSYS is also employed to provide reference solutions, considering a bi-dimensional approach using the PLANE223 element for piezoelectric layers. This element has eight nodes with up to five degrees of freedom per node. For the non-piezoelectric layers, the higher order (quadratic) element named PLANE183 is considered.

5.1. Convergence study of the proposed algorithm

The aim of the present section is to assess the performance of the proposed method to model coupling piezoelectric problems. In addition, a convergence study to evaluate the effect of the mesh size on spatial coordinates is addressed. For this purpose, a piezoelectric monomorph beam studied by Fernandes [51] is considered (see Fig. 3a). The monomorph beam is analysed assuming cylindrical bending (plane strain), for which the strains and the electric displacement in the y direction are considered to be negligible and therefore the columns and vectors in the 3D constitutive matrices associated to the negligible variables can be directly ignore. Different length to thickness ratios are tested for both close and open circuit electrical boundary conditions considering different spatial meshes. The monomorph is made of PZT-4 piezoelectric transversely isotropic ceramic. The characteristics of the test are described as follows:

- *Geometry*: thickness $h = 1\,\mathrm{mm}$ and three length to thickness ratios $S = L/h = 5, 10, 50$.
- *Material properties*:
  $\{C_{11}, C_{33}, C_{44}, C_{12}, C_{13}\} = \{139, 115, 25.6, 77.8, 74.3\}\,\mathrm{GPa}$,
  $\{e_{15}, e_{31}, e_{33}\} = \{12.7, -5.2, 15.1\}\,\mathrm{C/m^2}$,
  $\{\varepsilon_{11}, \varepsilon_{33}\} = \{13.06, 15.51\}\times 10^{-9}\,\mathrm{F/m}$, $\rho = 7550\,\mathrm{kg/m^3}$.

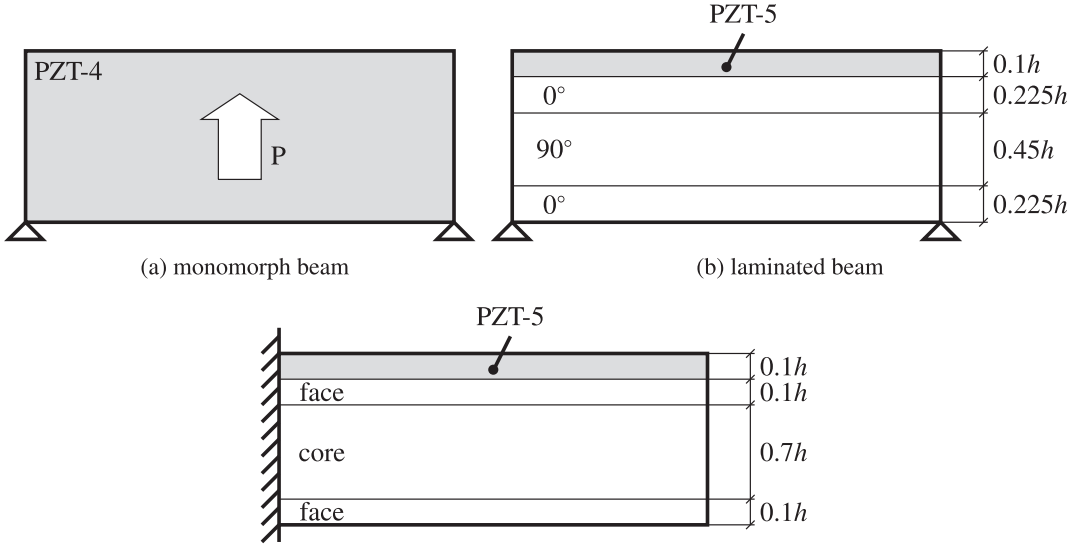

(a) monomorph beam

(b) laminated beam

(c) sandwich beam

Fig. 3. Beam tests configuration.

M. *Boundary conditions*: the beam is simply supported at its ends: $u_3 = 0\ \forall z$ (through the whole thickness). Two sets of electric boundary conditions are considered:
   - A close circuit or short circuit condition (SC), with the potential forced to remain zero (grounded) at the top and bottom surfaces of the monomorph beam.
   - An open circuit condition (OC), where the electric potential remains free everywhere.

In order to evaluate the convergence of the proposed methodology, a study with regard to the mesh size is carried out. The problem is evaluated by considering different meshes, with a number of n_z elements

Table 2
Convergence study for the first three natural frequencies of the monomorph beam. The reference ANSYS values are in Hz.

		SC frequency error (%)				OC frequency error (%)			
S	n_z	f_1	f_2	f_3	cum.	f_1	f_2	f_3	cum.
5	2	0.07	0.23	0.48	0.79	1.56	0.08	0.27	1.92
	4	0.03	0.07	0.10	0.20	0.21	0.06	0.03	0.30
	6	0.03	0.06	0.08	0.16	0.01	0.06	0.03	0.11
	8	0.03	0.05	0.07	0.16	0.01	0.06	0.05	0.13
	10	0.03	0.05	0.07	0.15	0.02	0.07	0.03	0.12
	2D model [51]	0.48	1.07	1.23	2.77	0.28	0.76	1.10	2.15
	ANSYS	**63910.9**	**219460**	**416755**	-	**64191.7**	**221862**	**422847**	-
10	2	0.02	0.06	0.13	0.21	0.01	0.04	0.10	0.15
	4	0.01	0.02	0.03	0.05	0.00	0.01	0.01	0.01
	6	0.01	0.01	0.03	0.05	0.05	0.01	0.01	0.07
	8	0.00	0.02	0.03	0.05	0.00	0.01	0.01	0.02
	2D model [51]	0.12	0.37	0.64	1.13	0.08	0.27	0.51	0.87
	ANSYS	**16797.2**	**63843.1**	**133694**	-	**16823.8**	**64185.4**	**134967**	–
50	1	0.01	0.03	0.07	0.11	0.01	0.03	0.07	0.11
	2	0.00	0.00	0.01	0.01	0.00	0.00	0.00	0.00
	2D model [51]	0.01	0.03	0.05	0.09	0.01	0.02	0.04	0.08
	ANSYS	**684.116**	**2730.13**	**6119.17**	-	**684.169**	**2730.95**	**6123.36**	–

Table 3
Open circuit (OC) dimensionless natural frequencies of simply support laminated beam.

S	Mode type	Exact 3D	Present	Error (%)	CRLT [52]	CRLT error (%)
5	*bend*	5.534	5.535	0.0	5.659	2.3
	bend	13.625	13.609	0.1	13.973	2.6
	bend	22.058	21.929	0.6	22.698	2.9
	bend	30.709	30.712	0.0	32.096	4.5
	bend	39.392	39.311	0.2	42.291	7.4
	bend	47.990	48.122	0.3	53.263	11.0
	t/c	37.203	37.219	0.0	38.091	2.4
	sh	–	37.337	–	37.634	–
	sh	58.447	58.450	0.0	61.708	5.6
10	*bend*	7.443	7.470	0.4	7.525	1.1
	bend	22.137	22.138	0.0	22.637	2.3
	bend	38.128	38.129	0.0	39.108	2.6
	bend	54.502	54.481	0.0	55.896	2.6
	bend	71.214	71.225	0.0	73.072	2.6
	bend	88.232	88.237	0.0	90.807	2.9
	t/c	78.293	78.266	0.0	78.846	0.7
	sh	–	149.389	–	150.533	–
	sh	177.107	176.418	0.4	178.656	0.9
20	*bend*	8.370	8.372	0.0	8.400	0.4
	bend	29.770	29.770	0.0	30.103	1.1
	bend	57.829	57.802	0.0	58.874	1.8
	bend	88.550	88.551	0.0	90.553	2.3
	bend	120.290	120.181	0.1	123.292	2.5
	bend	152.514	152.569	0.0	156.456	2.6
	t/c	159.334	159.341	0.0	159.641	0.2
	sh	–	595.256	–	602.129	–
	sh	627.418	627.449	0.0	631.793	0.7
100	*bend*	8.754	8.755	0.0	8.755	0.0
	bend	34.812	34.802	0.0	34.834	0.1
	bend	77.578	77.579	0.0	77.688	0.1
	bend	136.121	136.094	0.0	136.459	0.2
	bend	209.246	209.247	0.0	210.048	0.4
	bend	295.585	295.693	0.0	297.194	0.5
	t/c	801.586	801.587	0.0	801.651	0.0
	sh	14965.634	15057.896	0.6	15083.435	0.8

along the thickness. In the longitudinal domain, the size of the elements is the same as in the thickness direction for each analysis. The numerical values of the natural frequencies obtained with the PGD method by means of the Eq. (23) are compared with results computed with the commercial software ANSYS using a very refined mesh obtained after a convergence study and the two-dimensional model solutions from [51].

Table 2 presents the analysis of the first three bending natural frequencies for the very thick to very thin beams for both open and close circuit conditions. The values of the natural frequencies computed with ANSYS are taken as reference to calculate the relative errors of the solution obtained with the proposed algorithm.

It can be inferred from Table 2 that the convergence rate is rather high. In most cases it is only necessary to consider two numerical layers to obtain a value with a relative error below 1%. The PGD results show an excellent agreement with reference values, even closer to those obtained by the Fernandes 2D model which considers a larger mesh with no spatial separation.

5.2. Laminated beam

In this section, a symmetric composite cross-ply beam with a piezoelectric layer bonded to its top analyzed in references [41,52] is considered. The beam is depicted in Fig. 3b. The aim of this analysis is to assess the performance of the proposed method to model piezoelectric laminated beams with different length to thickness ratios, for both open and close circuit conditions. The characteristics of the tests are described as follows:

- *Geometry*: the lamination scheme is $[pz/0^\circ/90^\circ/0^\circ]$ with relative thickness of $0.1h/0.225h/0.45h/0.225h$, where pz indicates the piezoelectric layer. Four length to thickness ratios from thick to very thin beams are analysed: $S = 5, 10, 20, 100$.
- *Material properties*: The substrate of the beam is made of graphite-epoxy with the following properties $\{E_L, E_T, G_{LT}, G_{TT}\} = \{181, 10.3, 7.17, 2.87\}$ GPa, $\{\nu_{LT}, \nu_{TT}\} = \{0.28, 0.33\}$, $\rho = 1578\,\mathrm{kg/m^3}$ where subscripts L and T refer to the fiber and transverse direction respectively. The piezoelectric layer is made of PZT-5A transversely isotropic ceramic with the following properties:
  $\{E_1, E_3, G_{23}\} = \{61.0, 53.2, 21.1\}$ GPa, $\{\nu_{12}, \nu_{13}\} = \{0.35, 0.38\}$,
  $\{d_{31}, d_{33}, d_{15}\} = \{-171, 374, 584\} \times 10^{-12}\,\mathrm{m/V}$,
  $\{\varepsilon_{11}, \varepsilon_{33}\} = \{1.53, 1.50\} \times 10^{-8}\,\mathrm{F/m}$, $\rho = 7600\,\mathrm{kg/m^3}$.
- *Boundary conditions*: the beam is simply supported at its ends. Two sets of electric boundary conditions are considered for the inner surfaces:
  - An open circuit condition (OC), where the electric potential remains free everywhere, excepted on the inner surface of the piezoelectric layer where it is forced to be zero.
  - A close circuit or short circuit condition (SC), with the potential forced to remain zero (grounded) at the outer and inner surfaces of the piezoelectric layer.

The results of the natural frequencies are presented under a dimensionless value computed as $\bar{\omega} = \omega_n LS\sqrt{\rho_0/Y_0}$, with $\rho_0 = 1578\,\mathrm{kg/m^3}$ and $Y_0 = 10.3\,\mathrm{GPa}$ corresponding to the graphite-epoxy substrate. The vibration mode type is denoted as *bend*, *sh* and *t/c* for bending,

Table 4
Short circuit (SC) dimensionless natural frequencies of simply support laminated beam.

S	Mode type	Exact 3D	Present	Error (%)	CRLT [52]	CRLT error (%)
5	*bend*	5.517	5.536	0.3	5.643	2.3
	bend	13.589	13.599	0.1	13.943	2.6
	bend	22.002	21.914	0.4	22.645	2.9
	bend	30.635	30.712	0.3	32.010	4.5
	bend	39.307	39.311	0.0	42.164	7.3
	bend	47.901	48.023	0.3	53.095	10.8
	t/c	37.034	37.211	0.5	37.923	2.4
	sh	–	37.338	–	37.633	–
	sh	58.404	58.452	0.1	61.681	5.6
10	*bend*	7.412	7.443	0.4	7.496	1.1
	bend	22.066	22.138	0.3	22.572	2.3
	bend	38.020	38.129	0.3	39.015	2.6
	bend	54.355	54.480	0.2	55.772	2.6
	bend	71.027	71.225	0.3	72.908	2.6
	bend	88.006	87.992	0.0	90.593	2.9
	t/c	78.031	78.183	0.2	78.585	0.7
	sh	–	149.612	–	150.533	–
	sh	177.022	177.617	0.3	178.585	0.9
20	*bend*	8.331	8.372	0.5	8.361	0.4
	bend	29.648	29.771	0.4	29.982	1.1
	bend	57.620	57.802	0.3	58.676	1.8
	bend	88.264	88.551	0.3	90.290	2.3
	bend	119.930	120.181	0.2	122.973	2.5
	bend	152.080	152.778	0.5	156.083	2.6
	t/c	158.870	159.351	0.3	159.178	0.2
	sh	–	595.256	–	602.128	–
	sh	627.313	627.449	0.0	631.696	0.7
100	*bend*	8.711	8.754	0.5	8.712	0.0
	bend	34.640	34.784	0.4	34.664	0.1
	bend	77.202	77.579	0.5	77.313	0.1
	bend	135.474	136.114	0.5	135.813	0.2
	bend	208.269	209.252	0.5	209.074	0.4
	bend	294.235	295.598	0.5	295.849	0.5
	t/c	799.373	801.587	0.3	799.438	0.0
	sh	14965.520	14882.606	0.6	15083.327	0.8

shear and extensional modes, respectively. The numerical values obtained with the PGD method are compared with results computed with the coupled refined layerwise theory (CRLT) presented in [52], consisting of a coupled refined global–local finite element model for which all the kinematic and stress continuity conditions are satisfied at the layer interfaces in the presence of non-zero in plane electric field component. Exact three-dimensional elasticity solution shown in [52], which has been derived from the study by Heyliger and Brooks in 1995 [53], is taken as a reference.

Table 3 presents the values of the dimensionless natural frequencies for the thick to very thin beams, for the open circuit electrical condition. The first six bending frequencies as well as the extensional and shear modes are compared with the exact three-dimensional elasticity solution. These results show the excellent agreement with reference values for all types of modes. The maximum relative error is 0.6 %, although most of them are below 10^{-4} expressed in times one.

The values of the dimensionless natural frequencies for the thick to very thin beams for the close circuit electrical condition are shown in Table 4. The first six bending frequencies as well as the extensional and shear modes are also compared with the exact three-dimensional elasticity solution. In this instance, the maximum relative error is also 0.6 %, but in general these errors are higher than those obtained for the open circuit condition. In any case, the results show a very good fit with respect to the reference values and mainly improve those obtained with the coupled refined layerwise theory, especially for the thick case.

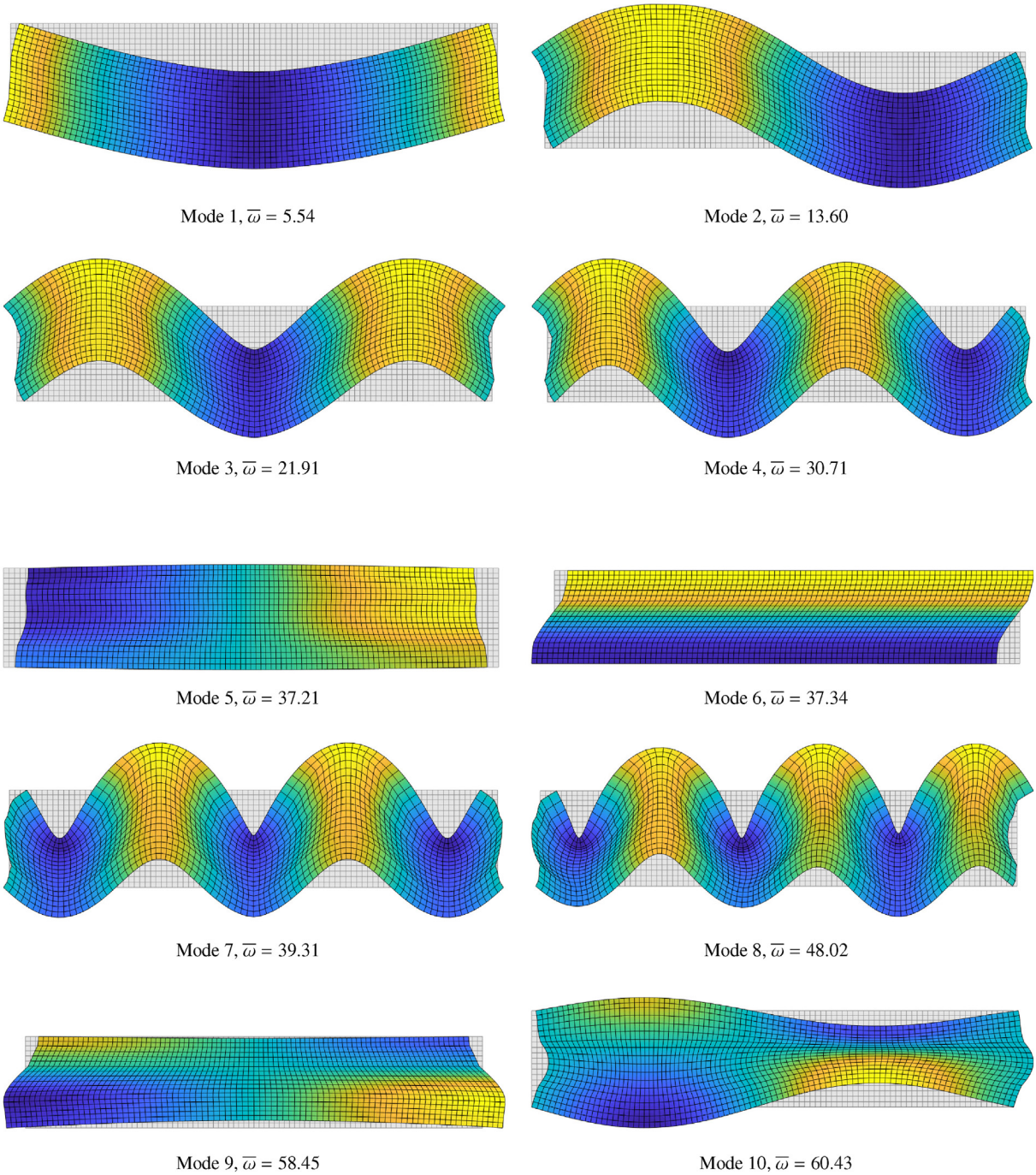

Fig. 4. PGD solution of modes shapes for the laminated beam ($pz/0°/90°/0°$) with $S = 5$, for short circuit condition.

Table 5
Open circuit dimensionless natural frequencies of simply support sandwich beam.

S	Mode type	Exact 3D	Present	Error (%)	CRLT [52]	CRLT error (%)
5	*bend*	3.974	3.974	0.01	4.258	7.1
	bend	8.962	8.963	0.01	9.153	2.1
	bend	14.344	14.353	0.07	13.291	7.3
10	*bend*	6.221	6.221	0.00	6.538	5.1
	bend	15.895	15.892	0.02	17.035	7.2
	bend	25.729	25.728	0.00	27.173	5.6
	bend	35.847	35.853	0.02	36.694	2.4
	bend	46.384	46.407	0.05	45.541	1.8
	bend	57.375	57.409	0.06	53.633	6.5
	sh	62.168	62.167	0.00	62.535	0.6
20	*bend*	7.866	7.877	0.14	8.026	2.0
	bend	24.883	24.880	0.01	26.154	5.1
	bend	44.087	44.084	0.01	47.082	6.8
	bend	63.581	63.574	0.01	68.148	7.2
	bend	83.159	83.155	0.00	88.739	6.7
	bend	102.916	102.918	0.00	108.747	5.7
	sh	131.774	131.776	0.00	132.315	0.4

Table 6
Open circuit dimensionless natural frequencies of cantilever sandwich beam.

S	Mode type	ANSYS	Present	Error (%)	CRLT [52]	CRLT error (%)
5	*bend*	1.880	1.885	0.3	1.989	5.8
	bend	6.144	6.181	0.6	6.433	4.7
	bend	11.618	11.732	1.0	11.436	1.6
	t-c	15.400	15.416	0.1	–	–
	bend	17.448	17.666	1.2	14.847	14.9
10	*bend*	2.592	2.595	0.1	2.670	3.0
	bend	9.987	10.019	0.3	10.624	6.4
	bend	20.393	20.467	0.4	21.656	6.2
	bend	30.165	30.524	1.2	31.289	3.7
	t-c	33.327	33.401	0.2	–	–
	bend	41.120	41.665	1.3	41.404	0.7
	bend	51.841	52.277	0.8	50.064	3.4
20	*bend*	2.967	2.968	0.0	2.997	1.0
	bend	14.661	14.678	0.1	15.299	4.3
	bend	32.959	33.018	0.2	34.951	6.0
	bend	52.321	52.450	0.2	55.911	6.9
	t-c	67.506	67.551	0.1	–	–
	bend	72.436	72.354	0.1	77.303	6.7
	bend	92.277	92.315	0.0	98.001	6.2

Table 7
Open circuit dimensionless natural frequencies of clamped sandwich beam.

S	Mode type	ANSYS	Present	Error (%)	CRLT [52]	CRLT error (%)
5	*bend*	4.849	4.858	0.2	5.152	6.3
	bend	9.995	10.087	0.9	10.055	0.7
	bend	15.700	15.748	0.3	14.332	8.6
10	*bend*	8.520	8.485	0.4	9.122	7.8
	bend	17.477	17.427	0.3	18.561	7.0
	bend	27.636	27.642	0.0	28.797	5.0
	bend	38.124	38.052	0.2	38.517	1.8
	bend	49.090	48.891	0.4	47.602	2.3
	bend	60.368	60.262	0.2	55.820	6.8
20	*bend*	13.534	13.452	0.6	14.181	5.6
	bend	29.351	29.215	0.5	31.228	7.1
	bend	47.751	47.550	0.4	50.990	7.5
	bend	67.019	66.753	0.4	71.473	7.3
	bend	86.793	86.452	0.4	91.982	6.6
	bend	106.895	106.617	0.3	112.103	5.5

Fig. 4 represents the first ten vibration modes for the thick beam considering short circuit condition. The PGD algorithm is able to detect not only bending modes, but also extensional, shear and thickness modes with complex displacement distribution along either the beam axis or the thickness.

5.3. Sandwich beam

In order to evaluate the PGD algorithm for solving coupled piezoelectric problems in sandwich beams with layers of very different characteristics, the present test consists of a three-layer sandwich beam composed of two graphite-epoxy faces and a soft core with a PZT-5A layer bonded to its top as shown in Fig. 3c. Additionally, the proposed formulation is validated to solve problems under different boundary conditions. This comprehensive test is also analysed in [41,52] with the following characteristics:

- *Geometry*: Thickness of the piezoelectric layer and face sheets are $0.1h$ while thickness of the core is assumed to be $0.7h$. Three length to thickness ratios are analysed: $S = 5, 10, 20$.
- *Material properties*: The face sheets are made of graphite-epoxy with the following properties
  $\{E_L, E_T, G_{LT}, G_{TT}\} = \{131.1, 6.9, 3.588, 2.3322\}$ GPa, $\{\nu_{LT}, \nu_{TT}\} = \{0.32, 0.49\}$, $\rho = 1000\,\mathrm{kg/m^3}$
  The material properties of the soft core are:
  $\{E_1, E_2, E_3, G_{12}, G_{13}, G_{23}\} = \{0.2208, 0.2001, 2760, 16.56, 545.1, 455.4\}$ MPa, $\{\nu_{12}, \nu_{13}, \nu_{23}\} = \{0.99, 0.00003, 0.00003\}$, $\rho = 70\,\mathrm{kg/m^3}$.
- *Boundary conditions*: Three different support cases are considered; simply support, cantilever and clamped, under open circuit electrical boundary conditions.

In Tables 5–7, the natural frequencies are also presented under a dimensionless value computed as $\bar{\omega} = \omega_n LS\sqrt{\rho_0/Y_0}$, with $\rho_0 = 1000\,\mathrm{kg/m^3}$ and $Y_0 = 6.9\,\mathrm{GPa}$. The numerical values obtained with the PGD method are compared with results of the coupled refined theory in [52] and the results computed with the commercial software ANSYS using a very refined mesh, except for the simply support case for which the exact 3D solution is also provided in the previous

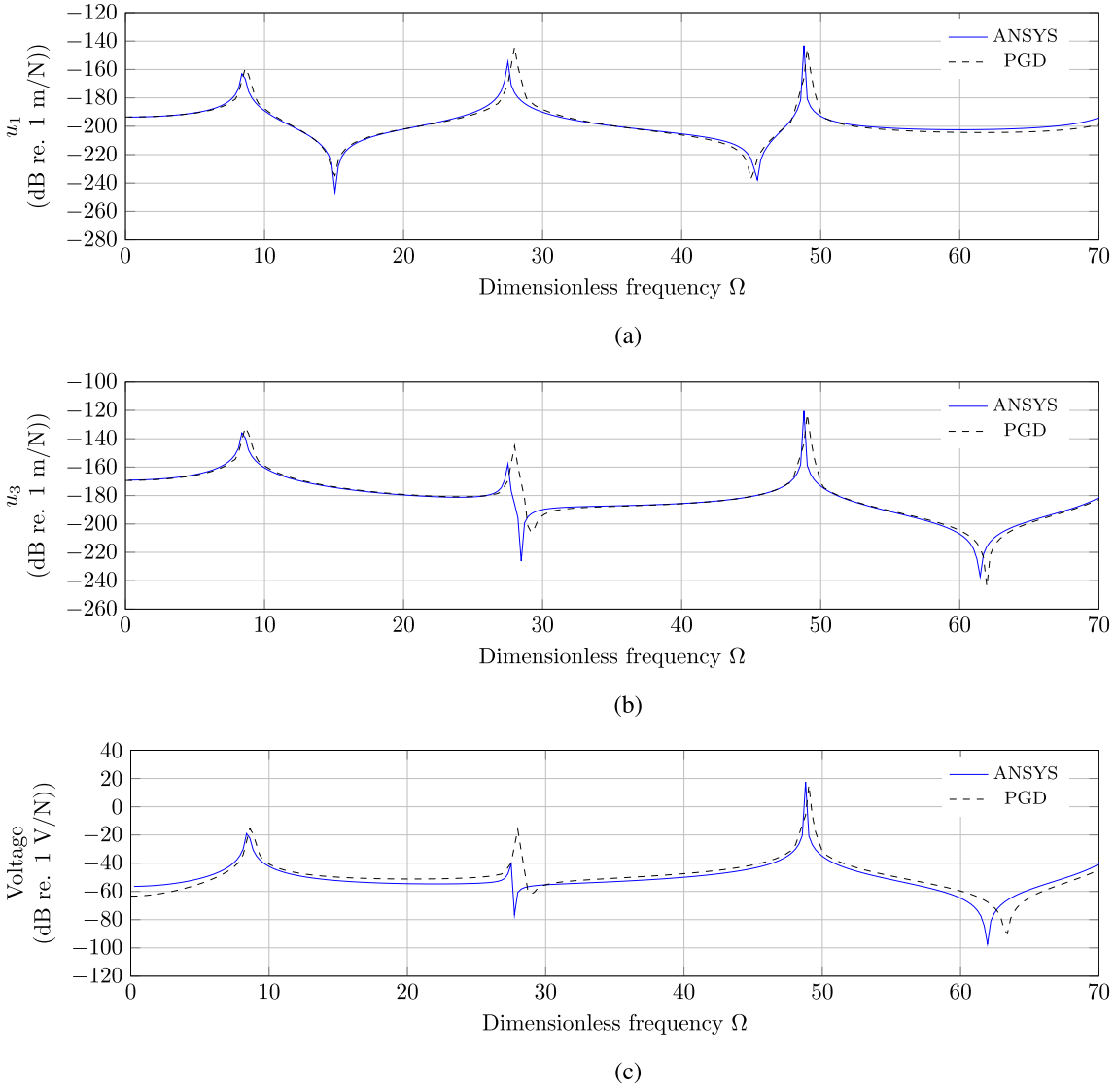

Fig. 5. FRF evaluated at the top at $x = L/3$ for the clamped sandwich beam with $S = 10$: (a) horizontal displacement, (b) vertical displacement (c) voltage.

reference. It should be mentioned here that for the cantilever and the clamped beam tests it is required to build simutaneously 2-tuple in order to achieve accurate results as in [54]. Further information on this technique can be also found in [55,56].

As a general remark, the highest frequencies occur for the clamped beam and the lowest values are obtained for the cantilever beam (clamped/free case). The natural frequencies obtained with the PGD method are almost always lower than those of the couple refined layerwise model with continuous inter-laminar stresses (CRLT) and the differences with the reference values remain always low. The maximum relative error is 1.3 % and the average relative error does not exceed 0.3 % for the three cases of boundary conditions considered. This is especially remarkable for the simply supported beam, for which the result of the PGD model achieves a really high accuracy compared to the exact three-dimensional elastic solution. In this case, the average error obtained with the PGD methodology is 0.02% while that achieved by the CRLT model is almost 5%.

Fig. 5 is designed to show the potential of the new robust variational formulation to find the solution for a set of the load frequency within an interval $[\omega_{min}, \omega_{max}]$. In the graph, the frequency response function (FRF) of the electromechanical problem is plotted. It shows the agreement between the amplitude of the displacements and the voltage response calculated both through a harmonic analysis in ANSYS and using the proposed PGD formulation. The semi-logarithmic representation allow us to detect the anti-resonance peaks. This particular feature can be used to evaluate the validity of the computed FRF using the PGD method. In particular, Fig. 5 represents the FRF of vertical and horizontal displacements and voltage separately, for the clamped sandwich beam under a vertical harmonic point load placed at $x = L/2$. Only the response at the top at $x = L/3$ of the beam with a slenderness ratio of $S = 10$ is represented. In this case, there are six bending modes in the frequency range under consideration, as it is remarked in Table 7. Nevertheless, only the symmetrical vibration bending modes (odd modes) can be distinguished in this graphical representation. This is due to the fact that the vibration nodes of the anti-symmetric bending modes (even modes) are located at the central line of the beam where the load is applied. The PGD results are in good concordance with ANSYS solution.

6. Conclusions

The main goal of this paper is to extend the PGD formulation to multi-field analysis in solid mechanics for the forced vibration problems. A new formulation based on the PGD method applied to bidimensional piezoelectric laminated beams is developed. A harmonic space-frequency description of the dynamic problem is first considered and a variable separation in the spatial domain is introduced. For both spatial coordinates x (beam axis coordinate) and z (thickness coordinate), a classical 3-node FE is used in the discretization. In addition, the load frequency is also introduced as a problem variable. The derived iterative methodology implies the computation of three 1D problems for each enrichment step used to represent the solution. The fixed-point method is employed to obtain the results for each of the N enrichment steps. The advantages of the proposed algorithm become relevant when the number of numerical layers increases and greater precision is required. In these cases the number of degrees of freedom in the classical formulation of the problem grows exponentially and the separation of variables becomes a very useful tool to reduce the order and limit the computational cost. Here, the potential of the PGD formulation has been demonstrated by the accuracy of its results.

Indeed, the proposed formulation has been validated through several numerical tests, including different composite and sandwich beam configurations with a great variety of slenderness ratios and boundary conditions. The current study show the potential of the approach to evaluate all kinds of mode shapes, including complex thickness modes with non-uniform displacement distribution along x and z axis. This is achieved by the layerwise approach. In addition, the method has been proved to be successful in detecting even small variations in natural frequencies derived from different electrical boundary conditions, such as short circuit and open circuit conditions. This opens up the possibility of confidently introducing electrical loads into the formulation, by adding an equivalent capacitance matrix to the dielectric matrix as in reference [57]. This would lead to the extension of the PGD approach to the parametric modeling of bimorph piezoelectric energy harvesting devices.

Funding support

This work was supported by the Universidad de Granada.

CRediT authorship contribution statement

María Infantes: Formal analysis, Software, Writing - original draft, Visualization. **Philippe Vidal:** Methodology, Formal analysis, Writing - review & editing. **Rafael Castro-Triguero:** Conceptualization, Resources, Supervision. **Laurent Gallimard:** Methodology, Formal analysis. **Olivier Polit:** Resources, Supervision.

Declaration of Competing Interest

The authors declare that they have no known competing financial interests or personal relationships that could have appeared to influence the work reported in this paper.

References

[1] Duarte A, Ferreira BL, Nóvoa PRO, Torres Marques A. Multifunctional material systems: a state-of-the-art review. Compos Struct 2016;151:3–35.
[2] Gibson R. A review of recent research on mechanics of multifunctional composite materials and structures. Compos Struct 2010;92(12):2793–810.
[3] Chopra I. Review of state of art of smart structures and integrated systems. AIAA J 2002;40(11):2145–87.
[4] Gaudenzi P. Smart structures: physical behaviour, mathematical modelling and applications. John Wiley & Sons Ltd; 2009.
[5] Zhang Z, Xiang H, Shi Z. Mechanism exploration of piezoelectric energy harvesting from vibration in beams subjected to moving harmonic loads. Compos Struct 2017;179:368–76.
[6] Lu Q, Liu L, Scarpa F, Leng J, Liu Y. A novel composite multi-layer piezoelectric energy harvester. Compos Struct 2018;201:121–30.
[7] Banerjee S, Roy S. A Timoshenko like model for piezoelectric energy harvester with shear mode. Compos Struct 2018;204:677–88.
[8] Akbar M, Curiel-Sosa JL. An iterative finite element method for piezoelectric energy harvesting composite with implementation to lifting structures under gust load conditions. Compos Struct 2019;219:97–110.
[9] Benjeddou A. Advances in piezoelectric finite element modeling of adaptive structural elements: a survey. Comput Struct 2000;76(1–3):347–63.
[10] Saravanos D, Heyliger P. Mechanics and computational models for laminated piezoelectric beams, plates, and shells. Appl Mech Rev 1999;52(10):305–19.
[11] Carrera E, Brischetto S, Nali P. Plates and shells for smart structures: classical and advanced theories for modeling and analysis. John Wiley & Sons Ltd; 2011.
[12] Vidal P, D'Ottavio M, Thaier MB, Polit O. An efficient finite shell element for the static response of piezoelectric laminates. J Intell Mater Syst Struct 2011;22(7):671–90.
[13] Crawley E, de Luis J. Use of piezoelectric actuators as element of intelligent structures. AIAA J 1987;25(10):1373–85.
[14] Tzou H, Gadre M. Theoretical analysis of a multi-layered thin shell coupled with piezoelectric shell actuators for distributed vibration controls. J Sound Vib 1989;132(3):433–50.
[15] Wang BT, Rogers C. Laminate plate theory for spatially distributed induced strain actuators. J Compos Mater 1991;25(4):433–52.
[16] Sung C, Chen T, Chen S. Piezoelectric modal sensor/actuator design for monitoring/generating flexural and torsional vibrations of cylindrical shells. J Vib Acoust 1996;118(1):48–55.
[17] Allik H, Hughes TJ. Finite element method for piezoelectric vibration. Int J Numer Meth Eng 1970;2(2):151–7.
[18] Tzou H, Tseng C. Distributed piezoelectric sensor/actuator design for dynamic measurement/control of distributed parameter systems: a piezoelectric finite element approach. J Sound Vib 1990;138(1):17–34.

[19] Xu K, Noor A, Tang Y. Three-dimensional solutions for coupled thermo-electro-elastic response of multi-layered plates. Comput Methods Appl Mech Eng 1995;126(3–4):355–71.
[20] Reddy J. An evaluation of equivalent-single-layer and layerwise theories of composite laminates. Compos Struct 1993;25(1–4):21–35.
[21] Suleman A, Venkaya V. A simple finite element formulation for a laminated composite plate with piezoelectric layers. J Intell Mater Syst Struct 1995;6 (6):776–82.
[22] Sheikh A, Topdar P, Halder S. An appropriate FE model for through-thickness variation of displacement and potential in thin moderately thick smart laminates. Compos Struct 2001;51(4):401–9.
[23] Wang S. A finite element model for the static and dynamic analysis of a piezoelectric bimorph. Int J Solids Struct 2004;41(15):4075–96.
[24] Chee C, Tong L, Steven P. A mixed model for composite beams with piezoelectric actuators and sensors. Smart Mater Struct 1999;8(3):417–32.
[25] Thornburgh R, Chattopadhyay A. Simultaneous modeling of mechanical and electrical response of smart composite structures. AIAA J 2002;40(8):1603–10.
[26] Fukunaga H, Hu N, Ren G. Finite element modeling of adaptive composite structures using a reduced higher-order plate theory via penalty functions. Int J Solids Struct 2001;38(48–49):8735–52.
[27] Mitchell J, Reddy J. A refined hybrid plate theory for composite laminates with piezoelectric laminae. Int J Solids Struct 1995;32(16):2345–67.
[28] Shu X. Free-vibration of laminated piezoelectric composite plates based on an accurate theory. Compos Struct 2005;67(4):375–82.
[29] Saravanos D, Heyliger P. Coupled layerwise analysis of composite beams with embedded piezoelectric sensors and actuators. J Intell Mater Syst Struct 1995;6 (3):350–63.
[30] Kusculuoglu Z, Fallahi B, Royston T. Finite element model of a beam with a piezoceramic patch actuator. J Sound Vib 2004;276(1–2):27–44.
[31] Semedo Garçao J, Mota Soares C, Mota Soares C, Reddy J. Analysis of laminated adaptive plate structures using layerwise finite element models. Comput Struct 2004;82(23–26):1939–59.
[32] Garcia Lage R, Mota Soares C, Mota Soares C, Reddy J. Analysis of adaptive plate structures by mixed layerwise finite elements. Compos Struct 2004;66 (1–4):269–76.
[33] Heyliger P, Ramirez G, Saravanos D. Coupled discrete-layer finite elements for laminated piezoelectric platess. Commun Numer Methods Eng 1994;10 (12):971–81.
[34] Saravanos D, Heyliger P, Hopkins D. Layerwise mechanics and finite element model for the dynamic analysis of piezoelectric composite plates. Int J Solids Struct 1997;34(3):359–78.
[35] Robaldo A, Carrera E, Benjeddou A. A unified formulation for finite element analysis of piezoelectric adaptive plates. Comput Struct 2006;84 (22–23):1494–505.
[36] Tzou H, Ye R. Analysis of piezoelastic structures with laminated piezoelectric triangle shell elements. AIAA J 1996;34(1):110–5.
[37] Ambartsumyan S. Theory of anisotropic plates. Technomic Publishing, Co., 1970..
[38] Carrera E. Historical review of zig-zag theories for multilayered plates and shells. Appl Mech Rev 2003;56(3):287–308.
[39] Oh J, Cho M. A finite element based on cubic zig-zag plate theory for the prediction of thermo-electric-mechanical behaviors. Int J Solids Struct 2004;41 (5–6):1357–75.
[40] Kapuria S. An efficient coupled theory for multilayered beams with embedded piezoelectric sensory and active layers. Int J Solids Struct 2001;38 (50–51):9179–99.
[41] Kapuria S, Alam N. Efficient layerwise finite element model for dynamic analysis of laminated piezoelectric beams. Comput Methods Appl Mech Eng 2006;195 (19–22):2742–60.
[42] Cho M, Oh J. Higher order zig-zag theory for fully coupled thermo-electric-mechanical smart composite plates. Int J Solids Struct 2004;41(5–6):1331–56.
[43] D'Ottavio M, Kropling B. An extension of reissner mixed varaitional theorem to piezoelectric laminates. Mech Adv Mater Struct 2006;13(2):139–50.
[44] Carrera E, Nali P. Mixed piezoelectric plate elements with direct evaluation of transverse electric displacement. Int J Numer Meth Eng 2009;80(4):403–24.
[45] Ammar A, Mokdada B, Chinesta F, Keunings R. A new family of solvers for some classes of multidimensional partial differential equations encountered in kinetic theory modeling of complex fluids. J Nonnewton Fluid Mech 2006;139(3):153–76.
[46] Savoia M, Reddy J. A variational approach to three-dimensional elasticity solutions of laminated composite plates. J Appl Mech 1992;59(2S):S166–75.
[47] Bognet B, Bordeu F, Chinesta F, Leygue A, Poitou A. Advanced simulation of models defined in plate geometries: 3D solutions with 2D computational complexity. Comput Methods Appl Mech Eng 2012;201:1–12.
[48] Vidal P, Gallimard L, Polit O. Proper generalized decomposition and layer-wise approach for the modeling of composite plate structures. Int J Solids Struct 2013;50(14–15):2239–50.
[49] Infantes M, Vidal P, Castro-Triguero R, Gallimard L, García-Macías E, Polit O. Forced vibration analysis of composite beams based on the variable separation method. Mech Adv Mater Struct 2021;28(6):618–34.
[50] Vidal P, Gallimard L, Polit O. Modeling of piezoelectric plates with variables separation for static analysis. Smart Mater Struct 2016;25(5):055043.
[51] Fernandes A, Pouget J. Modèle et étude de composants piézoélectriques: applications aux structures mulifonctionnelles. Ph.D. Thesis at University Paris VI, 2000..
[52] Beheshti-Aval SB, Lezgy-Nazargah M. Coupled refined layerwise theory for dynamic free and forced response of piezoelectric laminated composite and sandwich beams. Meccanica 2013;48(6):1479–500.
[53] Heyliger P, Brooks S. Exact free vibration of piezoelectric laminates in cylindrical bending. Int J Solids Struct 1995;32:2945–60.
[54] Vidal P, Gallimard L, Polit O. Free vibration analysis of composite plates based on a variable separation method. Compos Struct 2019;230:111493.
[55] Ammar A, Chinesta F. Circumventing curse of dimensionality in the solution of highly multidimensional models encountered in quantum mechanics using meshfree finite sums decomposition. In: Griebel M, Schweitzer MA, editors. Meshfree Methods for Partial Differential Equations IV Lecture Notes in Computational Science and Engineering, vol 65. Berlin, Heidelberg: Springer; 2008.
[56] Cancs E, Ehrlacher V, Lelivre T. Greedy algorithms for high-dimensional eigenvalue problems. Constr Approx 2014;40:387–423.
[57] Qin Z, Talleb H, Yan S, Xu X, Ren Z. Application of PGD on parametric modeling of a piezoelectric energy harvester. IEEE Trans Magn 2016;52(11):7210211.